New data on the earliest known arsinoitheriid embrithopod (Mammalia, Paenungulata), Namatherium from the middle Eocene of Namibia (project)

Emmanuel Gheerbrant, Guillaume Billet, Martin Pickford

▶ **To cite this version:**

Emmanuel Gheerbrant, Guillaume Billet, Martin Pickford. New data on the earliest known arsinoitheriid embrithopod (Mammalia, Paenungulata), Namatherium from the middle Eocene of Namibia (project). Geodiversitas, 2025, 47 (8), pp.343-366. ⟨10.7934/P5894⟩. ⟨mnhn-05354485⟩

HAL Id: mnhn-05354485

https://mnhn.hal.science/mnhn-05354485v1

Submitted on 7 Nov 2025

HAL is a multi-disciplinary open access archive for the deposit and dissemination of scientific research documents, whether they are published or not. The documents may come from teaching and research institutions in France or abroad, or from public or private research centers.

L'archive ouverte pluridisciplinaire **HAL**, est destinée au dépôt et à la diffusion de documents scientifiques de niveau recherche, publiés ou non, émanant des établissements d'enseignement et de recherche français ou étrangers, des laboratoires publics ou privés.

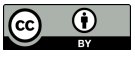

Distributed under a Creative Commons CC BY 4.0 - Attribution - International License

geodiversitas

2025 • 47 • 8

New data on the earliest known arsinoitheriid embrithopod (Mammalia, Paenungulata), *Namatherium* Pickford, Senut, Morales, Mein & Sanchez, 2008 from the middle Eocene of Namibia

Emmanuel GHEERBRANT, Guillaume BILLET & Martin PICKFORD

art. 47 (8) — Published on 22 May 2025
www.geodiversitas.com

PUBLICATIONS SCIENTIFIQUES

MUSÉUM NAL HIST NATURELLE

Directeur de la publication / *Publication director* : Gilles Bloch,
Président du Muséum national d'Histoire naturelle

Rédacteur en chef / *Editor-in-chief*: Didier Merle

Assistant de rédaction / *Assistant editor*: Emmanuel Côtez (geodiv@mnhn.fr)

Mise en page / *Page layout*: Emmanuel Côtez

Comité scientifique / *Scientific board*:
Christine Argot (Muséum national d'Histoire naturelle, Paris)
Beatrix Azanza (Museo Nacional de Ciencias Naturales, Madrid)
Raymond L. Bernor (Howard University, Washington DC)
Henning Blom (Uppsala University)
Gaël Clément (Muséum national d'Histoire naturelle, Paris)
Ted Daeschler (Academy of Natural Sciences, Philadelphie)
Cédric Del Rio (Muséum national d'Histoire naturelle)
Gregory D. Edgecombe (The Natural History Museum, Londres)
Ursula Göhlich (Natural History Museum Vienna)
Jin Meng (American Museum of Natural History, New York)
Brigitte Meyer-Berthaud (CIRAD, Montpellier)
Zhu Min (Chinese Academy of Sciences, Pékin)
Isabelle Rouget (Muséum national d'Histoire naturelle, Paris)
Sevket Sen (Muséum national d'Histoire naturelle, Paris, retraité)
Stanislav Štamberg (Museum of Eastern Bohemia, Hradec Králové)
Paul Taylor (The Natural History Museum, Londres, retraité)

Couverture / *Cover*:
Réalisée à partir des Figures de l'article/*Made from the Figures of the article*.

Geodiversitas est indexé dans / Geodiversitas *is indexed in:*
– Science Citation Index Expanded (SciSearch®)
– ISI Alerting Services®
– Current Contents® / Physical, Chemical, and Earth Sciences®
– Scopus®

Geodiversitas est distribué en version électronique par / Geodiversitas *is distributed electronically by:*
– BioOne® (http://www.bioone.org)

Les articles ainsi que les nouveautés nomenclaturales publiés dans *Geodiversitas* sont référencés par /
Articles and nomenclatural novelties published in Geodiversitas *are referenced by:*
– ZooBank® (http://zoobank.org)

Geodiversitas est une revue en flux continu publiée par les Publications scientifiques du Muséum, Paris
Geodiversitas *is a fast track journal published by the Museum Science Press, Paris*

Les Publications scientifiques du Muséum publient aussi / *The Museum Science Press also publish:* ***Adansonia***, ***Zoosystema***, ***Anthropozoologica***, ***European Journal of Taxonomy***, ***Naturae***, ***Cryptogamie*** **sous-sections** ***Algologie***, ***Bryologie***, ***Mycologie, Comptes Rendus Palevol***

Diffusion – Publications scientifiques Muséum national d'Histoire naturelle
CP 41 – 57 rue Cuvier F-75231 Paris cedex 05 (France)
Tél. : 33 (0)1 40 79 48 05 / Fax : 33 (0)1 40 79 38 40
diff.pub@mnhn.fr / http://sciencepress.mnhn.fr

© Publications scientifiques du Muséum national d'Histoire naturelle, Paris, 2025
ISSN (imprimé / *print*) : 1280-9659/ ISSN (électronique / *electronic*) : 1638-9395

New data on the earliest known arsinoitheriid embrithopod (Mammalia, Paenungulata), *Namatherium* Pickford, Senut, Morales, Mein & Sanchez, 2008 from the middle Eocene of Namibia

Emmanuel GHEERBRANT
Guillaume BILLET
Martin PICKFORD
CR2P (CNRS, MNHN, Sorbonne Université), Département Origines et Évolution,
Muséum national d'Histoire naturelle, case postale 38,
57 rue Cuvier, F-75231 Paris cedex 05 (France)
emmanuel.gheerbrant@mnhn.fr (corresponding author)
guillaume.billet@mnhn.fr
martin.pickford@mnhn.fr

Submitted on 22 April 2024 | accepted on 26 August 2024 | published on 22 May 2025

urn:lsid:zoobank.org:pub:A6CE8243-0BB3-4526-85A2-B5ADFD54D883

Gheerbrant E., Billet G. & Pickford M. 2025. — New data on the earliest known arsinoitheriid embrithopod (Mammalia, Paenungulata), *Namatherium* Pickford, Senut, Morales, Mein & Sanchez, 2008 from the middle Eocene of Namibia. *Geodiversitas* 47 (8): 343-368. https://doi.org/10.5252/geodiversitas2025v47a8. http://geodiversitas.com/47/8

ABSTRACT
We here describe and interpret recently discovered material of the embrithopod mammal *Namatherium blackcrowense* Pickford, Senut, Morales, Mein & Sanchez, 2008 from the Lutetian Black Crow locality, in Namibia, a species previously only known from the holotype. The new specimen, a distal part of a skull including the petrosals, complements the holotype well and allows a virtual reconstruction of a large part of the skull of *N. blackcrowense*. The CT scan study of the petrosal and labyrinth and the squamosal morphology unambiguously support referral of the new specimen to *N. blackcrowense.* Our comparisons and phylogenetic study support a close relationship between *Namatherium* Pickford, Senut, Morales, Mein & Sanchez, 2008 and the more derived Fayum genus *Arsinoitherium* Beadnell, 1902, and its inclusion within the family Arsinoitheriidae. This is evidenced by remarkable shared derived traits of the petrosal and inner ear such as the thick and flattened semicircular canals, the absent *fossa subarcuata*, the reduced secondary bony lamina, the secondary *crus commune* in the course of separation, and the partially fused *fenestra cochleae* and cochlear aqueduct. They add to previous arsinoitheriid synapomorphies reported on the holotype such as presence of nasal horns and the pseudolophodont molars. *Namatherium* helps to reconstruct the ancestral morphotype of the family Arsinoitheriidae, and it emphasises the advanced condition of *Arsinoitherium zitteli* Beadnell, 1902 with respect to *Namatherium* in many autapomorphic traits, especially in striking reversals in some cranial morphological traits. This implies a substantial divergent evolution of the *Arsinoitherium* clade between the Lutetian and Priabonian, which remains undocumented and poorly understood from an adaptive perspective.

KEY WORDS
Africa,
Namibia,
Black Crow,
Lutetian,
Mammalia-
Embrithopoda,
Arsinoitheriidae,
Namatherium,
skull anatomy,
petrosals,
CT scan.

RÉSUMÉ
Nouvelles données sur le plus ancien embrithopode arsinoitheriidé (Mammalia, Paenungulata), Namatherium *Pickford, Senut, Morales, Mein & Sanchez, 2008 de l'Éocène moyen de Namibie.*
Nous rapportons la récente découverte d'un nouveau matériel du mammifère embrithopode *Namatherium blackcrowense* Pickford, Senut, Morales, Mein & Sanchez, 2008 de la localité lutétienne de Black Crow, en Namibie, une espèce auparavant seulement connue par l'holotype. Le nouveau spécimen, correspondant à la partie postérieure d'un crâne avec les deux pétreux, complète bien l'holotype et permet la reconstitution virtuelle d'une grande partie du crâne de *N. blackcrowense*. L'étude CT scan du pétreux et du labyrinthe osseux, de même que la morphologie du squamosal, appuient sans ambiguïté l'appartenance du nouveau spécimen à *N. blackcrowense*. Nos comparaisons et notre étude phylogénétique confirment la proche parenté de *Namatherium* Pickford, Senut, Morales, Mein & Sanchez, 2008 avec le genre plus dérivé du Fayoum, *Arsinoitherium* Beadnell, 1902, et son appartenance à la famille des Arsinoitheriidae. Cela est soutenu par plusieurs caractères dérivés communs remarquables du pétreux et de l'oreille osseuse interne tels que les canaux semi-circulaires épais et aplatis, la *fossa subarcuata* absente, la lamine osseuse secondaire réduite, la *crus commune* secondaire en cours de séparation, et la *fenestra cochleae* et l'aqueduc cochléaire partiellement fusionnés. Ceux-ci s'ajoutent aux synapomorphies d'arsinoithériidés auparavant identifiées sur l'holotype de *Namatherium*, telles que la présence de cornes nasales et de molaires pseudolophodontes. *Namatherium* permet de reconstruire le morphotype ancestral de la famille des Arsinoitheriidae, et souligne la condition dérivée d'*Arsinoitherium zitteli* Beadnell, 1902 par rapport à *Namatherium* dans de nombreux caractères autapomorphiques, dont plusieurs reversions crâniennes remarquables. Cela implique une grande divergence évolutive de la lignée d'*Arsinoitherium* entre le Lutétien et le Priabonien qui reste inconnue et mal comprise sur le plan adaptatif.

MOTS CLÉS
Afrique,
Namibie,
Black Crow,
Lutétien,
Mammalia-
Embrithopoda,
Arsinoitheriidae,
Namatherium,
anatomie crânienne,
pétreux,
CT scan.

INTRODUCTION

The Black Crow fossiliferous locality in the Northern Sperrgebiet, Namibia (Fig. 1), has yielded a rich middle Eocene (Lutetian) vertebrate fauna including one of the most diversified mammal faunas known from the Palaeogene of sub-Saharan Africa (Pickford *et al.* 2008a). The mammalian assemblage is dominated by endemic African taxa such as hyaenodonts, hystricomorph and anomaluroid rodents (Pickford 2018b), a megachiropteran, two African primates (an adapiform and a possible simiiform), some of the earliest known insectivorous afrotherians (chrysochlorids, potamogalids, tenrecids) (Pickford 2019b, 2019c), and paenungulates such as hyracoids (Pickford 2018a, 2018f) and an embrithopod (Pickford *et al.* 2008a). It has also yielded a reithroparamyid rodent of North American affinities (Mein & Pickford 2018), an adapisoriculid "insectivore" (Pickford 2019a), and other "insectivores" (Morales & Pickford 2018).

We herein describe and interpret new cranial material of a large paenungulate from the locality that is referred to the embrithopod family Arsinoitheriidae Andrews, 1904 and to the species *Namatherium blackcrowense* Pickford, Senut, Morales, Mein & Sanchez, 2008 previously known from the same site, but only by the holotype (Pickford *et al.* 2008a). Fossils of the embrithopod family Arsinoitheriidae are known from fewer than a dozen localities in Afro-Arabia (Fig. 1) and at most of these localities only a few teeth or fragments of post-cranial bones are represented (Pickford 1986, 2015b; Sanders *et al.* 2004; Rasmussen & Gutierrez 2009; Zalmout *et al.* 2010; Vialle *et al.* 2013; Bamford & Pickford 2021). The exception is the Fayum, Egypt, which yielded abundant well-preserved skulls, mandibles and other skeletal material (Beadnell 1902; Andrews 1906). The discovery of additional skull material of the Lutetian genus *Namatherium* Pickford, Senut, Morales, Mein & Sanchez, 2008 is important, because it provides a more secure basis for making comparisons with *Arsinoitherium* Beadnell, 1902, and other African embrithopods such as *Stylolophus* Gheerbrant, 2018 from Morocco (Gheerbrant *et al.* 2021). Other embrithopods of the North Tethyan family Palaeoamasiidae Şen & Heintz, 1979 remain poorly known, with only jaws and dental remains present in available collections.

The new arsinoithere specimen from Black Crow preserves parts of the neurocranium that permits a detailed comparative anatomical study of the petrosal, inner ear, occipital region and related areas that were previously unknown in *Namatherium*.

MATERIAL AND METHODS

Scan, modelisation and software

The petrosal of the new specimen GSN BC 21'19 of *Namatherium blackcrowense* was investigated using high-resolution X-ray µCT at the AST-RX platform of the MNHN, Paris, using a GE Sensing and Inspection Technologies phoenix|x-

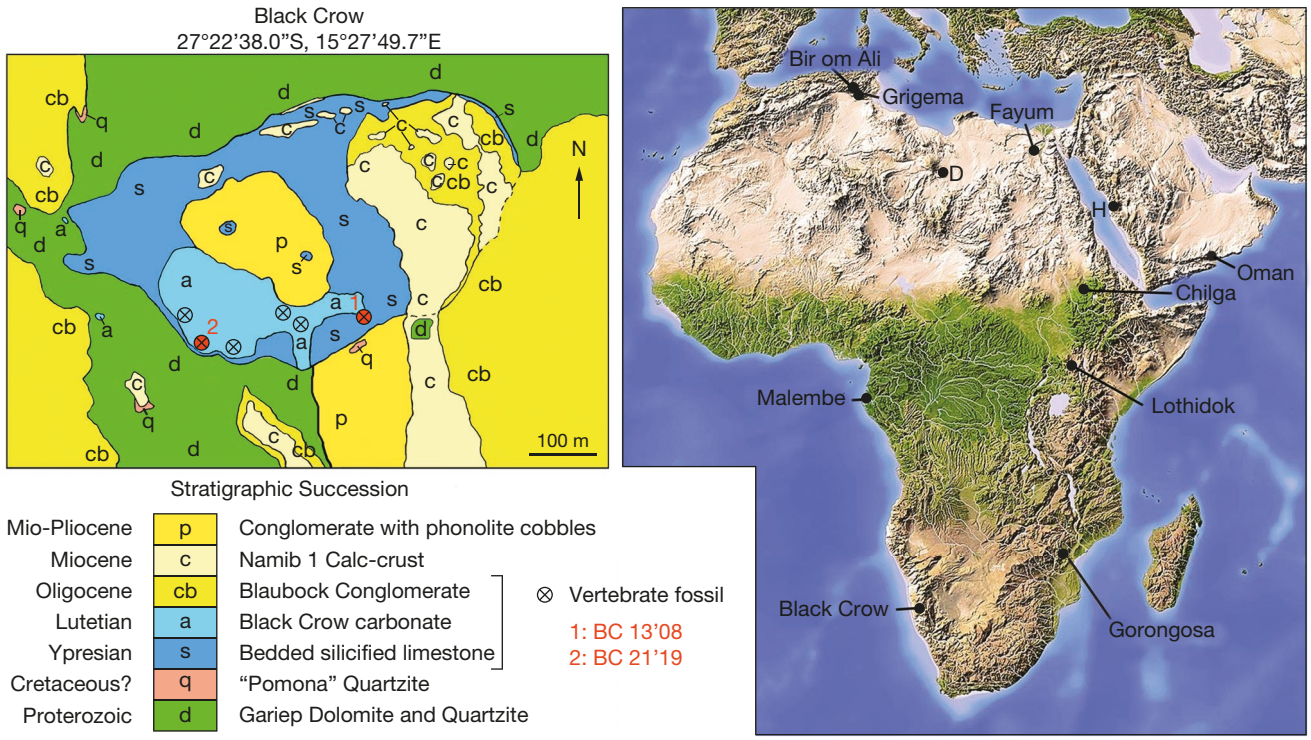

FIG. 1. — Geology of the Black Crow depression, Sperrgebiet, Namibia, detailing the discovery loci of cranial specimens of *Namatherium blackcrowense* Pickford, Senut, Morales, Mein & Sanchez, 2008. Map modified from Pickford *et al.* (2008b). Mobile sands are not shown on the map. The map of Africa and Arabia shows the localities from which large arsinoitheres have been collected (**D**, Dor el Talha; **H**, Harrat al Ujayfa). The Oman occurrences are at Taqah and Thaytiniti.

ray v|tome|x L240-180 CT scanner, with a resolution of 0.02234299 mm (voxel size). Data were reconstructed using datos|x reconstruction software (Phoenix|x-ray, release 2.0) and then exported into 16-bit TIFF images. We used the softwares Materialise Mimics® (release 11.1, 2017), Avizo 7.1.1 (Visualization Science Group) and MeshLab-67-bit-fp v2016.12 for the analysis, 3D modelisation, visualisation and measurement of the image stack and 3D Models.

Measurements and orientation

The petrosal and bony labyrinth of the inner ear were oriented using the *fenestra vestibuli* as a reference for the lateral orientation. The orientation indicated in the figure corresponds to the predominant orientation axes. The general protocol for measuring the bony labyrinth of *Namatherium blackcrowense* follows Gheerbrant *et al.* (2020: fig. 2). We have specified in the text the cases where our measurements are taken differently. Most measurements (length, area and volume) were made on the 3D digital model of the petrosals and labyrinths, using both Meshlab and Mimics.

The cochlear volume was obtained by separating the cochlear part from the vestibular part; measurement of the cochlear volume includes the proximal extremity of the cochlear canal (just proximal to the *f.vestibuli*) but it excludes the cochlear fossula, the aqueducts and the nerve tracts. The cochlear length was measured on the ventral surface of the canal and at its central lumen; it starts below the *fenestra vestibuli* (as for the volume measurement) and ends at the apex of the cochlea. The stapedial ratio was calculated following Segall (1970) as L/W, with L = length and W = width of the *fenestra vestibuli*. Calculation of the cochlear curvature and measurement of the number of turns of the cochlea follow the protocol of West (1985). The aspect ratio of the cochlea was calculated with the formula of Ekdale & Rowe (2011): H/W, with H = height and W = width of the cochlea.

Using MIMICS, we measured the inner ear height (IEH) following Billet *et al.* (2015) as the linear distance between the dorsal apex of the *crus commune* and the ventral apex of the cochlea. We calculated the ratio of the mean radius of curvature of the semicircular canals (SC) to the inner ear height (IEH), as a way of measuring the proportion of the semicircular canals at the inner ear scale. Calculation of the radii of curvature of the semicircular canals uses the Spoor–Zonneveld equation (Spoor & Zonneveld 1998): R = (L + W)/2) × 0.5, with L = length and W = width of the canals. Height and width of the semicircular canals were calculated from the center of the canal to the vestibule (which includes the ampullae) and following the protocol of Macrini *et al.* (2010). Length of the semicircular canals was measured on the 3D Models of the labyrinth at their mid width (projection of center of lumen) (e.g. Benoit *et al.* 2013b), either including or excluding the ampulla. We calculated the thickness ratio for both the semicircular canals and the *crus commune* as the section radius divided by the canal length (thin part, excluding ampulla) × 100 (Schmitt 2016; Gheerbrant *et al.* 2020). This ratio expresses quantitatively the global thickness of the canals; thin semicircular

canals have a thickness ratio lower than 3, stocky semicircular canals have a thickness ratio as high as, or higher than 3. A stocky *crus commune* has a thickness ratio as high as, or higher than 15 (Schmitt 2016). We calculated the angle variance index from 90° of the three semicircular canals of *Namatherium* following Malinzak *et al.* (2012) and Ruf *et al.* (2016) as Log 90var, with var = mean of the variance from 90° of the three semicircular canals. Using the software Geomagic (3D Systems Geomagic Wrap 2021), we defined planes for the ASC, PSC, LSC, cochlear canal basal turn and a line along the common crus to measure the angles between these structures. At least three points were placed to define each plane, which were computed using the "best fit" plane option. For the ASC, PSC and LSC, which are rather planar in *Namatherium*, points were placed on the outer aspect of the arc, at the orthogonal projection of the center of the lumen, which was determined graphically. For the cochlear basal turn, points were placed on the dorsal surface of the canal, at the orthogonal projection of the center of the canal. For the common crus, the line was traced on the medial aspect of the common crus at the orthogonal projection of the center of this duct. Angles between these elements were then measured using the plane-to-plane or line-to-plane options in Geomagic.

Cladistic analysis

We investigated the relationships of *Namatherium* based on a cladistic analysis with TNT 1.6 (Goloboff & Catalano 2016) and using the character matrix of Gheerbrant (2023) with some modifications given in Appendix 1. Our matrix modifications include the addition of new characters observed in the inner ear preserved in the specimen GSN BC 21'19 studied here, and corrections of several character states for *Pezosiren* Domning, 2001 following Domning *et al.* (2017), and for *Moeritherium* Andrews, 1901 following Benoit *et al.* (2023). In addition, with respect to Gheerbrant (2023) the terminal taxon Hyracoidea Huxley, 1869 is deleted, and replaced by the stem hyracoids *Seggeurius* Mahboubi, Ameur, Crochet & Jaeger, 1986, *Microhyrax* Sudre, 1979, *Dimaitherium* Barrow, Seiffert & Simons, 2010, and *Saghatherium antiquum* Andrews & Beadnell, 1902, all four coded as individual terminal taxa. The analysed character matrix includes 41 taxa and 212 characters, of which 38 are additive and nine are uninformative. The character numbering used in our description of our most parsimonious trees (MPTs) starts from 0 (default option in TNT). We developed a standard analysis with the Traditional Search command and using the TBR swapping algorithm (number of replicates 10, tree saved per replicate 100, memory 10 000 trees). The most parsimonious trees (MPTs) resulting from this analysis are provided as the strict consensus tree and the majority rule tree. For these analyses the default collapsing rule was changed to "max. length = 0". Bremer support values (BM) were calculated for 10 additional steps, and Bootstrap values were calculated from 100 tree replicates. The phylogenetic matrix used here is provided in the supplementary material (Appendix 2).

Abbreviations

Institutional abbreviation

GSN BC	Collection of the Geological Survey of Namibia, Black Crow locality.

Cladistic analysis

BM	Bremer support;
RI	retention index;
CI	consistency index;
MPT	most parsimonious tree.

Anatomical abbreviations

ASC	anterior semicircular canal;
LSC	lateral semicircular canal;
PSC	posterior semicircular canal;
SC	semicircular canals.

Measurements

L	length;
W	width.

GEOLOGICAL AND PALAEOECOLOGICAL CONTEXTS

The fossil material studied here was collected by the Namibia Palaeontology Expedition in the Black Crow site, Northern Sperrgebiet of Namibia (Pickford *et al.* 2008a, b). The Black Crow site corresponds to limestone that accumulated in a small depression eroded into Proterozoic dolomites of the Gariep Group (Fig. 1). The lowermost deposits in the depression comprise well-bedded silicified limestones considered to be sub-aerial tuffs related to the Ystervark volcanic activity in the nearby Klinghardt Mountains (Pickford 2015a). These well-bedded deposits are overlain by fossiliferous freshwater limestones - the Black Crow carbonates. These limestones are overlain unconformably by the Blaubock Conglomerate of Rupelian age, and by a series of Miocene to Recent deposits (Fig. 1).

The cranial remains of *Namatherium blackcrowense* were collected from the Black Crow freshwater limestones in association with a diversity of invertebrates and vertebrates, as well as plant remains (fruits, roots). The mammalian fauna indicates a Lutetian correlation, although, given the great distance of Black Crow from other fossiliferous deposits of approximately equivalent age in Africa (the Maghreb, Libya, Egypt), it is not possible to determine the age more precisely.

The fossil landsnails from Black Crow (Pickford 2018e) indicate that the basin lay within in a temperate climatic zone with a summer rainfall regime (as opposed to a winter rainfall regime). The fossil fishes (Pickford 2018d) indicate that the water flowing within the basin was fresh and well-oxygenated. The presence of a fruit bat (pteropodid megachiropteran), as well as two primates species (an adapid and a simiiform), indicates that there were open or perhaps dense forests. The presence of fruits of the plant *Celtis* L. (Pickford 2018c) does not throw much light on the palaeoenvironment, because this plant survives today in a wide variety of ecosystems ranging from forest to semi-arid zones.

SYSTEMATIC PALAEONTOLOGY

Supercohort AFROTHERIA Stanhope, Waddell, Madsen, De Jong, Hedges, Cleven, Kao & Springer, 1998
Superorder PAENUNGULATA Simpson, 1945
Mirorder TETHYTHERIA McKenna, 1975
Order EMBRITHOPODA Andrews, 1906
Family ARSINOITHERIIDAE Andrews, 1904
Genus *Namatherium*
Pickford, Senut, Morales, Mein & Sanchez, 2008

Namatherium blackcrowense
Pickford, Senut, Morales, Mein & Sanchez, 2008
(Figs 2-11)

TYPE MATERIAL. — **Holotype. Namibia** • 1 specimen (partial skull); Namibia, Sperrgebiet, Black Crow; Lutetian; GSN BC 13'08 (Pickford *et al.* 2008a).

DIAGNOSIS. — See Pickford *et al.* (2008a).

TYPE LOCALITY AND AGE. — Black Crow, Sperrgebiet, Namibia. Lutetian in Pickford *et al.* (2008a).

REFERRED MATERIAL (new material). — GSN BC 21'19, posterior part of skull (basicranium) including right squamosal (two fragments), basioccipital, exoccipital, supraoccipital and left and right petrosals.

MEASUREMENTS. — See Tables 1-5.

DESCRIPTION

We here describe the new cranial specimen GSN BC 21'19 from Black Crow, which is attributed to *Namatherium blackcrowense* based on shared characters (see Discussion). GSN BC 21'19 consists of a damaged basicranium and posterior part of a skull comprising the squamosal, occipital and petrosal that are broken apart into seven pieces of bone. Each of these pieces of bone was reassembled and mounted in association with the holotype (partial skull) using their 3D digital models, which allowed the reconstruction of a large part of the skull of *Namatherium blackcrowense*, with the exception of the snout, the dorsal part of the skull and the lower jaw (Fig. 11 and Appendix 3).

We used anatomical terminology that generally follows the English equivalents of terms from the Nomina Anatomica Veterinaria, 5th edition (Waibl *et al.* 2005). When this practice was not possible (see Wible 2010), terms were taken from the general comparative literature cited below. Anatomical comparisons were made and detailed especially with *Arsinoitherium*, among other paenungulates.

Squamosal

The right squamosal is preserved as two broken fragments that retain anatomical connection at the level of the zygomatic process (Fig. 2). One piece of bone includes part of the zygomatic process with the posterior parts of the glenoid fossa and postglenoid process, and the most lateral part (roof) of the external auditory meatus (Fig. 2A, B). The other piece corresponds to the posterior part of the squamosal fragment with the external auditory meatus and the posttympanic process (Fig. 2C-F). The squamous part (scale) of the squamosal is missing (broken).

TABLE 1. — Measurements of the cochlea and fenestrae of the bony labyrinth of *Namatherium blackcrowense* Pickford, Senut, Morales, Mein & Sanchez, 2008, specimen GSN BC 21'19 (mm and mm³).

	Right lab.	Left lab.
Volume of the labyrinth	159.48	–
Volume of cochlea (excluding f. vestibuli and cochlear fossula)	–	64
Volume of vestibule + semicircular canals	88.90	–
IEH Inner Ear Height	13.8	13.47
Number of coils	1.75 (630°)	1.69 (610°)
Relative volume of the cochlea	44.4 %	–
Length of cochlear canal at central lumen	24.76	24.88
Length of *lamina secundaria*	7.54	7.27
Stapedial ratio	1.85	1.78
Angle of cochlear plan and *crus commune* (= vestibulo-cochlear angle; obtuse angle)	136.4°	132.3°
Angle of cochlear plan and LSC plan (acute angle)	52.5°	53.7°
Aspect ratio	0.51	0.50
Max Width of cochlea (diameter)	6.52	6.55
Max Height of cochlea	3.35	3.30
Length of cochlear aqueduct	8.35	7.86
Length of vestibular aqueduct	15.7	–

TABLE 2. — Dimensions (mm) of the semicircular canals of *Namatherium blackcrowense* Pickford, Senut, Morales, Mein & Sanchez, 2008, specimen GSN BC 21'19.

	Right lab.	Left lab.
Length of ASC with ampulla (without)	17.96 (15.4)	18.33 (15.51)
Length of PSC with ampulla (without)	18.78 (14.7)	18.91 (15.67)
Length of LSC with ampulla (without)	18 (16.01)	17.95
Angle ASC/PSC	89.44°	89.72°
Angle ASC/LSC	81.49°	83.41°
Angle PSC/LSC	85.31°	83.53°
Length of *crus commune*	5.1	5.5
Crus commune section radius	1.28	1.30

TABLE 3. — Width (**W**) and height (**H**) of the semicircular canals of *Namatherium blackcrowense* Pickford, Senut, Morales & Sanchez, 2008, specimen GSN BC 21'19 (in mm; measurement extending to mid canal section).

	ASC W	ASC H	Ratio ASC	PSC W	PSC H	Ratio PSC	LSC W	LSC H	Ratio LSC
Left labyrinth	7.37	7.37	1	6.74	7.07	0.95	5.47	6.55	0.84
Right labyrinth	7.33	7.36	1	6.6	7.27	0.91	5.13	6.51	0.79

The fragment of squamosal corresponding to the posterior part of the zygomatic process (Fig. 2A, B) perfectly matches in size and shape with the same area preserved in the holotype of *N. blackcrowense* (Fig. 11). It preserves most of the postglenoid process, but only a small part of the glenoid fossa corresponding to its most posterior and lateral part (Fig. 2B). As in the holotype, the postglenoid process forms a smooth low and inflated ridge behind the glenoid fossa. It extends transversely for about 55 mm. The glenoid fossa is shallow and flat as in the holotype, and it is open laterally. The overall construction of the zygomatic process of the squamosal is stout, with a very thick bone supporting the glenoid fossa (height between postglenoid process and upper part of the zygomatic process = 42 mm). As in the holotype, the zygo-

matic process flares strongly laterally, in contrast to that of *Arsinoitherium* Beadnell, 1902. Dorsal to the glenoid fossa, part of the crest of the zygomatic arch is preserved in the area close to the junction with the nuchal crest.

The other squamosal fragment (Fig. 2C-F) preserves the large and deep notch of the external auditory meatus, flanked by both the base of the postglenoid process and the posttympanic process. It also preserves on the dorsal side the posterior part of the temporal fossa (labelled "temp f" in Fig. 2D-F) and the damaged area of connection between the zygomatic and nuchal crests (Fig. 2D). The external auditory meatus is very deep and wide open ventrally. It is set very high, being located at least 55 mm above the postglenoid apophysis and glenoid fossa. Its closeness in height relative to the zygomatic crest of the squamosal indicates it was located higher than the orbits. This is displayed in our reconstruction of the skull (Fig. 11). The external auditory meatus is narrow anteroposteriorly (anteroposterior length =14 mm) but long transversally (transverse length = at least 64 mm). In lateral view it has a typical reversed U-shape. The broken medial side of the posterior wall of the postglenoid process shows the large (estimated diameter 4.6 mm) and long postglenoid canal in section (Fig. 2E). It opens as a postglenoid foramen at the mid height of the external auditory meatus. The medial position of the postglenoid foramen is shared with proboscideans (Tassy 1981; Gheerbrant *et al.* 2005). The postglenoid canal extends dorsally up to the roof of the external auditory meatus. More dorsally and anteriorly there is a (slightly less) large canal within the bone which is more or less parallel to the postglenoid canal; it might be homologous to the *canalis temporalis* described in proboscideans (Tassy, 1981) and to the posttemporal canal in other placentals. The posttemporal canal conveys *diploetica magna* vessels and, in mammals, is typically located between the lateral surface of the *pars canalicularis* of the petrosal and the overlying squamosal (Wible 2008; Muizon *et al.* 2015; MacPhee *et al.* 2021). This canal is independent of the postglenoid canal, which suggests that *Namatherium* has indeed both an intracranial opening of the posttemporal canal and an external and ventral postglenoid foramen. Posterior to the external auditory meatus, the posttympanic process is large and stout. It shows on its posterior side a bony suture with the exoccipital (Fig. 2E, F). The nuchal (= lambdoid) crest is damaged; it is barely visible on the back of the right squamosal fragment bearing the external auditory meatus and the posttympanic process. In this area, the nuchal crest seems to comprise mostly the squamosal, rather than the occipital.

Occipitals

The occipitals are preserved as three large and thick fragments of bones (Fig. 3): the basioccipital together with the occipital condyles, the exoccipitals preserving distinctly the dorsal margin of the foramen magnum, and a damaged fragment of the supraoccipitals. In the reconstruction assembling the isolated bones (Fig. 11), the occipital side of the skull is canted anteriorly.

Posterior to the external auditory meatus, the right squamosal fragment displays a suture with the right exoccipital which is partly preserved. In this area, the exoccipital is a bony tuberosity slightly inflated ventrally (Fig. 2C, E, F); it is homologous in position to the paroccipital process seen in *Arsinoitherium* at the ventro-lateral corner of its occiput (e.g., Andrews 1906, pl. I: "p.p."). It extends ventral to the postglenoid foramen level. However, the paroccipital process remains small in *Namatherium,* as in *Arsinoitherium*.

A damaged fragment of supraoccipital (maximal dimensions as preserved 52x46 mm), which lacks cortical bone, is present in the new material of *Namatherium blackcrowense* herein described (Fig. 3E, F). It probably corresponds to the upper part of the exoccipital bone, and it preserves only cancellous bone and the internal cerebellar surface. The cerebellar surface of the supraoccipital is characterised by the presence of a double median and longitudinal bony ridge which separates two smooth and elongated concave fossae (Fig. 3E) probably corresponding to endocasts of the cerebellum (separated in two lateral parts, possibly by cast of median vermis).

Exoccipital

A large fragment of the lower part of the exoccipitals is broken away as a single thick bony plate lacking the condyles. Its surface is more or less smooth, with low relief. The suture of the exoccipital with the supraoccipital is poorly preserved, and the occipital suture is not distinguishable. The exoccipital bone is comprised of one median concave surface, flanked by two oblique lateral surfaces that are inclined anteriorly. There is a very smooth median ridge of bone (nuchal tuberosity; minimum length 35 mm) that extends vertically from above the foramen magnum (Fig. 3C), likely for attachment of the *ligamentum nuchae*. This bony ridge is only weakly pronounced and much smaller than in *Arsinoitherium*. The median concave surface of the occipital bone is bounded laterally at mid height by a symmetrical bony tuberosity on both right and left sides.

The foramen magnum opens dorsally entirely in the exoccipitals, as in *Arsinoitherium*. The preserved dorsal part of the foramen magnum is high and narrow (minimum height and width, respectively 12 mm and 27 mm). It has a triangular outline (reversed V-shape) in contrast to the U-shape in *Arsinoitherium.* In the skull reconstruction, the foramen magnum faces posteriorly and its dorsal border arcs dorsally well above the condylar level. The occipital condyles are attached to the basioccipital fragment, instead of to the exoccipital one (Fig. 3A, B) but the sutures are not visible and these structures were most likely comprised of the exoccipitals, as usual in mammals. They are large, more widely separated and much less pedunculate and posteriorly prominent than in *Arsinoitherium*. The minimal intercondylar transverse length is 15 mm, which is 4 times smaller than in *Arsinoitherium*. The maximal intercondylar width, also known as the occipital condyle width (OCW, see Engelman 2022), is 92.8 mm. Most parts of the occipital condyles are located lower than the basioccipital. Caudally, the long axis of the condyles is oblique dorsolateral. They are narrow and shaped liked an ovoid cylinder (slightly more convex medially); this is different from

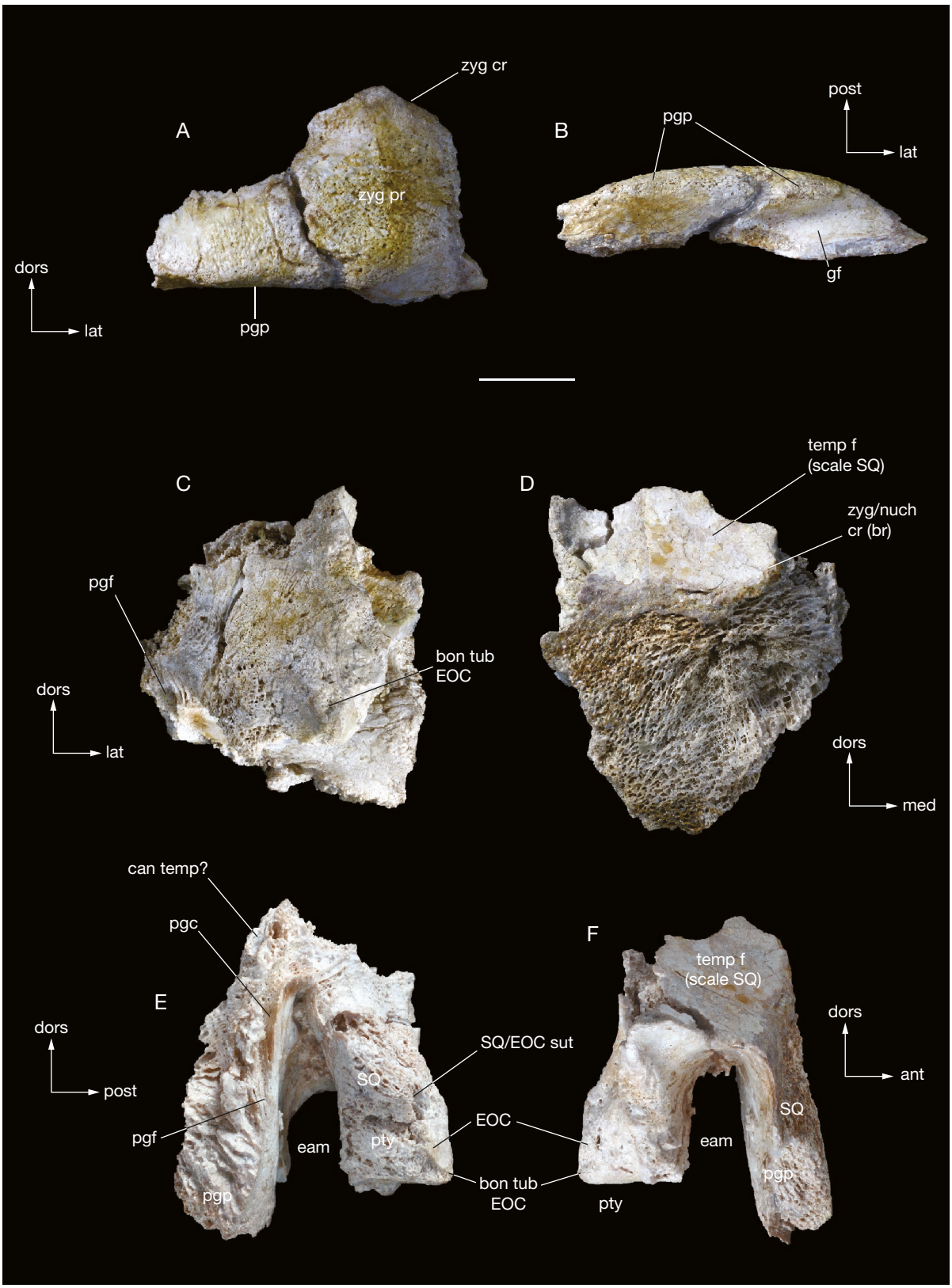

FIG. 2. — Right squamosal of *Namatherium blackcrowense* Pickford, Senut, Morales, Mein & Sanchez, 2008, referred specimen GSN BC 21'19 (photographs): **A**, **B**, part of the zygomatic process in posterior and ventral views, **C**-**F**, part of the external auditory meatus (postglenoid process and posttympanic process) in posterior, anterior, medial and lateral views. Abbreviations: **bon tub**, bony tuberosity of exoccipital; **can temp**, canalis temporalis; **eam**, external auditory meatus; **EOC**, exoccipital: **gf**, glenoid fossa; **pgc**, postglenoid canal; **pgf**, postglenoid foramen; **pgp**, postglenoid process; **pty**, posttympanic process; **SQ**, squamosal; **sut**, suture; **temp f**, temporal fossa (scale of the squamosal); **zyg cr** (**br**), zygomatic crest of the squamosal (broken); **zyg pr**, zygomatic process. Orientation axes: **dors**, dorsal; **med**, medial; **lat**, lateral; **post**, posterior. Photos by P. Loubry (CR2P, MNHN). Scale bar: 20 mm.

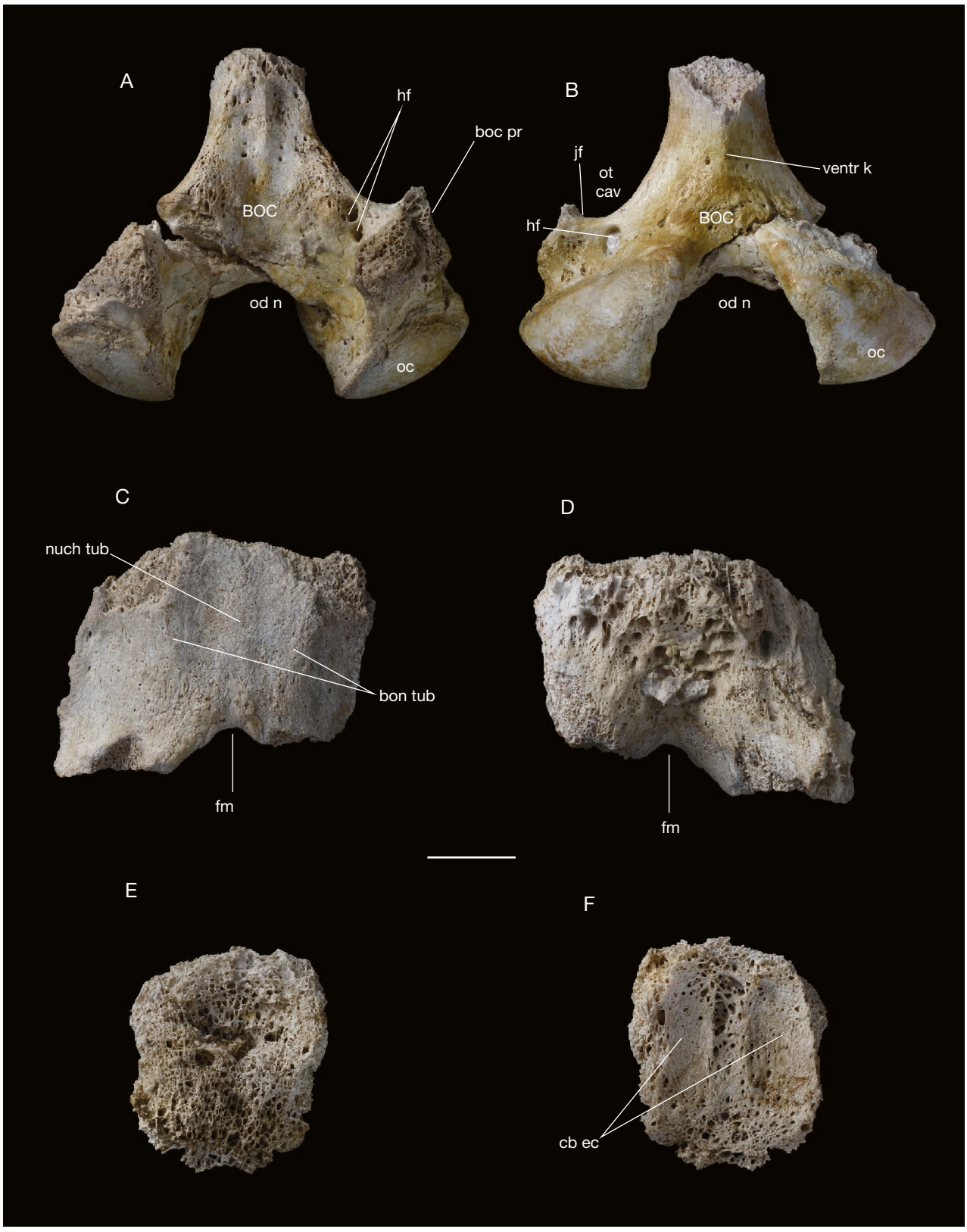

FIG. 3. — Occipital of *Namatherium blackcrowense* Pickford, Senut, Morales, Mein & Sanchez, 2008, referred specimen GSN BC 21'19 (photographs): **A**, **B**, basioccipital with attached occipital condyles in dorsal and ventral views; **C**, **D**, supraoccipital, lower part, in posterior and anterior (internal) views; **E**, **F**, supraoccipital, damaged upper part, in posterior and anterior (internal) views. Abbreviations: **Boc pr**, basioccipital process for attachment of the posttympanic process of squamosal; **bony tub**, bony tuberosity; **cb ec**, cerebellum endocasts; **fm**, foramen magnum; **hf**, hypoglossal foramen; **jf**, jugular foramen; **Nuch tub**, nuchal tuberosity; **Oc**, occipital condyle; **od n**, odontoid notch of the foramen magnum; **ot cav**, otic cavity (place of the petrosal); **vent k**, ventral keel. Photos by P. Loubry (CR2P, MNHN). Scale bar: 20 mm.

Arsinoitherium in which the condyles are subvertical, rounded, convex and dilated dorso-ventrally. In ventral view (Fig. 3A, B), the condyles have the shape of a right-angled triangle with the long oblique side oriented anteriorly. The articular surface of the condyles is extended dorsally and ventrally, and more so on the ventral side. In ventral view the articular surface of the occipital condyles is significantly shorter than in *Arsinoitherium*, being less expanded anteriorly.

Basioccipital

The ventral border of the foramen magnum (odontoid notch) consists of the basioccipital. It is wide (~35.5 mm) and deep (26 mm). In ventral view, the basioccipital is notched laterally on both sides by a wide and long otic cavity which lodged the petrosal. The large extent of the otic vacuity, at least on the medial side (the only preserved part neighbouring the petrosal), indicates that the petrosal was weakly connected with surrounding bones of the basicranium, similar to *Arsinoitherium* (Court 1992b). Posterolaterally in this vacuity, there is a smooth but distinct notch for the jugular foramen, which was open medially, as is visible on the right side of the fragment. More posteriorly, there is a large hypoglossal (condylar) foramen (l = 7.5 mm; w = 4.5 mm), in contrast to *Arsinoitherium* which lacks it. It has an oval outline with a longitudinal long axis and is composed dorsally of two openings and canals that are also visible on the dorsal surface of the basioccipital. On the lateral side, and better preserved on the right side, in front of the condyle, there is a basioccipital process for attachment to the posttympanic process of the squamosal. The ventral condyloid (hypoglossal) fossa between this basioccipital process and the condyles is not deep and is bounded posteriorly by an antero-medial crest of the condyles.

In front of the condyles, the anterior portion of the basioccipital narrows rapidly, forming a rod-like bone as in *Arsinoitherium*. At its anteriomost part, it is slightly higher (28.5 mm) than wider (22.5 mm) but not as much as in *Arsinoitherium*. The dorsal surface of the basioccipital is more or less flat and it bears a well-developed median bony ridge in its anterior part. The ventral surface bears a median bony keel that fades out about 12 mm in front of the condyles and about five millimetres anterior to the posterior edge of the otic vacuity.

Petrosal (Figs 4-9)

Both the right and left petrosals are present in the specimen GSN BC 21'19. The petrosal was loosely attached to the occipital and did not contact the basioccipital (see the vacuity described above) due to its small size relative to the skull, as in most large mammals. This is probably the result of a negative allometric growth of this bone relative to the rest of the cranium in mammals (its size increases at a lesser rate than that of the overall cranium; see Billet *et al.* 2015).

Since direct indication for the connection of the petrosal to preserved parts of the rest of the cranium are lacking (bone broken), the orientation of these bones in the following description is tentatively based on patterns commonly observed in mammals (e.g., *fenestra vestibuli* facing laterally). This orientation is further supported by the presence of a remnant of the surface of connection with the exoccipital, which is best preserved and visible on the left petrosal and faces medially (to posteromedially) (Fig. 5B)

Middle ear (Figs 4-7)

The petrosal of *Namatherium* is characterised by the presence of a large and flat medially extended epitympanic wing that is larger than the promontorium. It is likely that part of this wing is missing anteriorly, since the uneven anterior edge of the preserved portion is suggestive of a fracture. The preserved part of the epitympanic wing is plate-like, but there are two small longitudinal ridges extending across its surface from the lateral sides of the promontorium. The medialmost of these ridges corresponds to the mesial extension of the rostral tympanic process seen on the promontorium, and might be its homologue.

Tympanic (ventral) view. The promontorium (*pars cochlearis*) is inflated, rounded and ovoid. The rostral tympanic process is present but not strongly pronounced. As in *Arsinoitherium* the surface of the promontorium is smooth. It lacks any osteological feature (e.g., sulcus) that would be indicative of a transpromontorial course of the internal carotid artery (MacPhee & Forasiepi 2022). There is no medial flange of the promontorium.

The *fenestra vestibuli* is large and oval (stapedial ratio = 1.81; mean of right and left petrosals) in *Namatherium*. *Arsinoitherium* has a rounder *fenestra vestibuli* than *Namatherium* with a stapedial ratio of 1.6 (Benoit *et al.* 2013b), in a condition hitherto considered more derived among eutherians (e.g., Court 1992b; Ekdale 2013; but see discussion in Ruf *et al.* 2016). The proximal base of the *fenestra vestibuli*, at the cochlear canal junction, is constricted with respect the outer part of *fenestra vestibuli* (Fig. 9B, asterisk). In addition, it is oriented along an axis that is slightly oblique, i.e. it faces slightly more dorsally than the outer part of the *fenestra vestibuli* (Fig. 9B, arrow). Posterior to the *fenestra vestibuli* and just lateral to the facial sulcus is a well-developed and deep depression, corresponding to the stapedial fossa. It has an elongated, oval or teardrop outline. The external aperture of the cochlear fossula which encloses the *fenestra cochleae* is subcircular and larger than the *fenestra vestibuli*. It is vertical and faces posteriorly, being barely visible in tympanic view; this shape and orientation of the cochlear fossula is shared with *Prorastomus* and early proboscideans, and it was considered by Court (1990) to be derived among placentals, although the condition of an external aperture of the cochlear fossula facing posteriorly is found in most placentals. The *crista interfenestralis* is broad between the *fenestra vestibuli* and cochlear fossula and continues posteriorly as a sharp ridge posteromedial to the stapedial fossa. The cochlear aqueduct (*aquaeductus cochleae*) opens more dorsally and medially than the external aperture of the cochlear fossula. The presence of a cochlear aqueduct is plesiomorphic with respect to *Arsinoitherium* in which it is merged with the *fenestra cochleae*, forming a single perilymphatic foramen. The cochlear aqueduct is located at a distance of about 8 mm from the external aperture of the cochlear fossula in *Namatherium*.

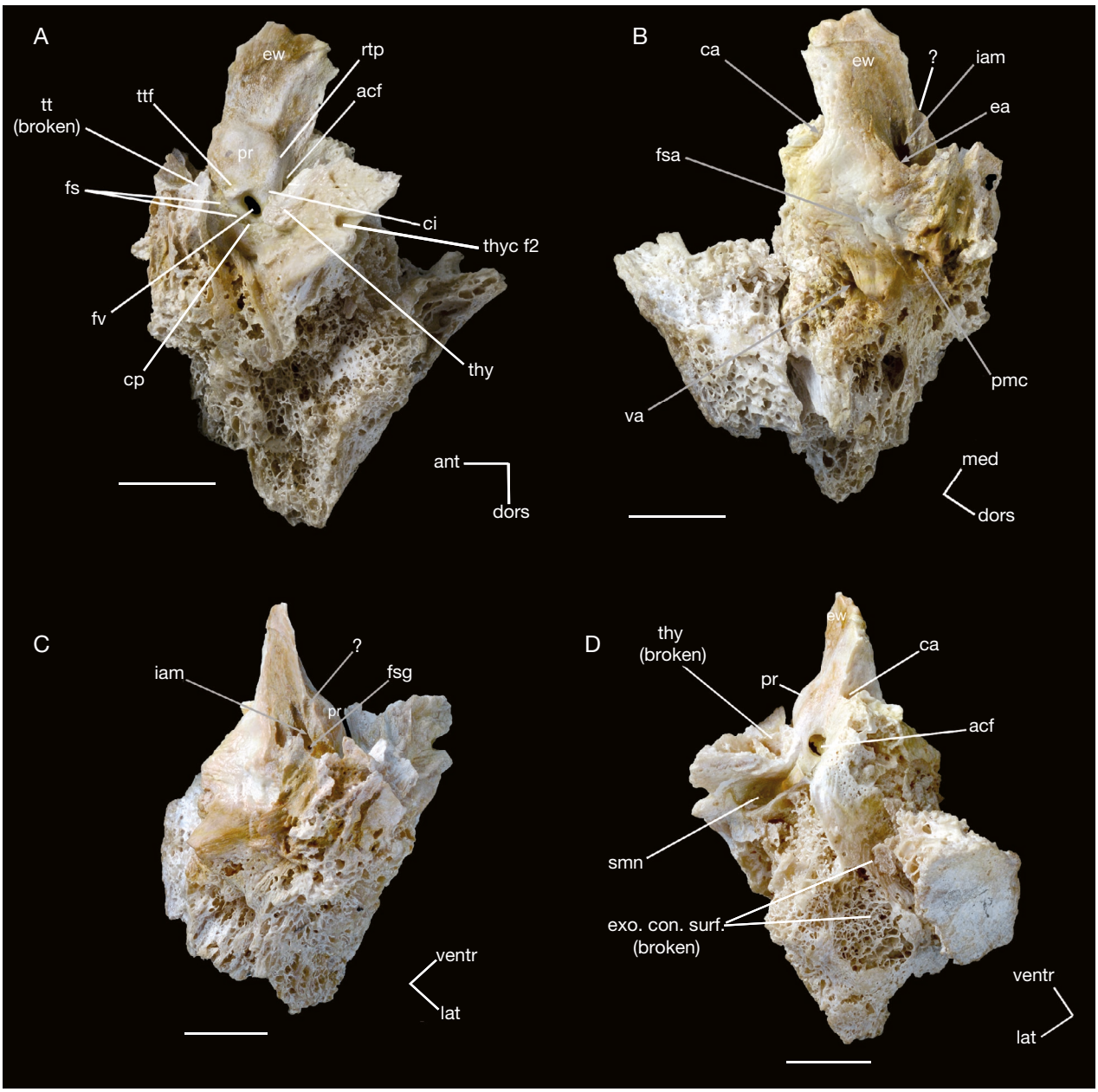

FIG. 4. — Right petrosal of *Namatherium blackcrowense* Pickford, Senut, Morales, Mein & Sanchez, 2008, referred specimen GSN BC 21'19 (photographs): **A**, lateral view; **B**, posteromedial view; **C**, anterior view; **D**, posterior view. Abbreviations for petrosal morphology: **acf**, external aperture of the cochlear fossula; **ca**, cochlear aqueduct; **ci**, crista interfenestralis; **cp**, crista parotica; **ea**, eminantia arcuata; **exo. con. surf. (broken)**, connecting surface of the right petrosal bone with the exoccipital; **ew**, epitympanic wing; **fs**, facial sulcus; **fsa**, *fossa subarcuata*; **fsg**, foramen singular; **fv**, *fenestra vestibuli*; **iam**, internal auditory meatus; **pmc**, petromastoid canal; **pr**, promontorium; **rtp**, rostral tympanic process; **smn**, stylomastoid notch; **thy**, tympanohyal; **thyc f2**, tympanohyal canal, posterolateral foramen; **tt**, tegmen tympani; **ttf**, tensor tympanic fossa; **va**, vestibular aqueduct. Orientation axes: **ant**, anterior; **dors**, dorsal; **med**, medial; **lat**, lateral; **post**, posterior; **ventr**, ventral. Photos by P. Loubry (CR2P, MNHN). Scale bars: 10 mm.

Lateral to the promontorium, the floor of the *cavum supracochleare*, which encloses the geniculate ganglion of the facial nerve (Voit, 1909), is broken on both petrosals, leaving apparent the entire course of the facial sulcus. The latter is wide and runs from the primary facial foramen (the outline of which is not preserved due to breakage in this area) anteriorly to the stylomastoid notch posteriorly. The secondary facial foramen is barely distinct, due to the breakage of the *cavum supracochleare*, but it might have opened slightly anterior to the *fenestra vestibuli* at the level of a crest marking the posterior edge of the tensor tympani fossa. Although most of the extent of this fossa must have lain on the *cavum supracochl*eare, a slight depression extending anteroposteriorly on the promontorium just anterior to the *fenestra vestibuli* is suggestive of its presence. The facial sulcus is bordered laterally by a high *crista parotica* joining the base of the tegmen tympani anteriorly and that of the tympanohyal posteriorly. The tympanohyal is large relative to the entire petrosal, which recalls a condition seen in other large mammals (e.g., rhinos, astrapotheres; G.B. pers. obs.). The tegmen tympani is present but broken on both petrosals.

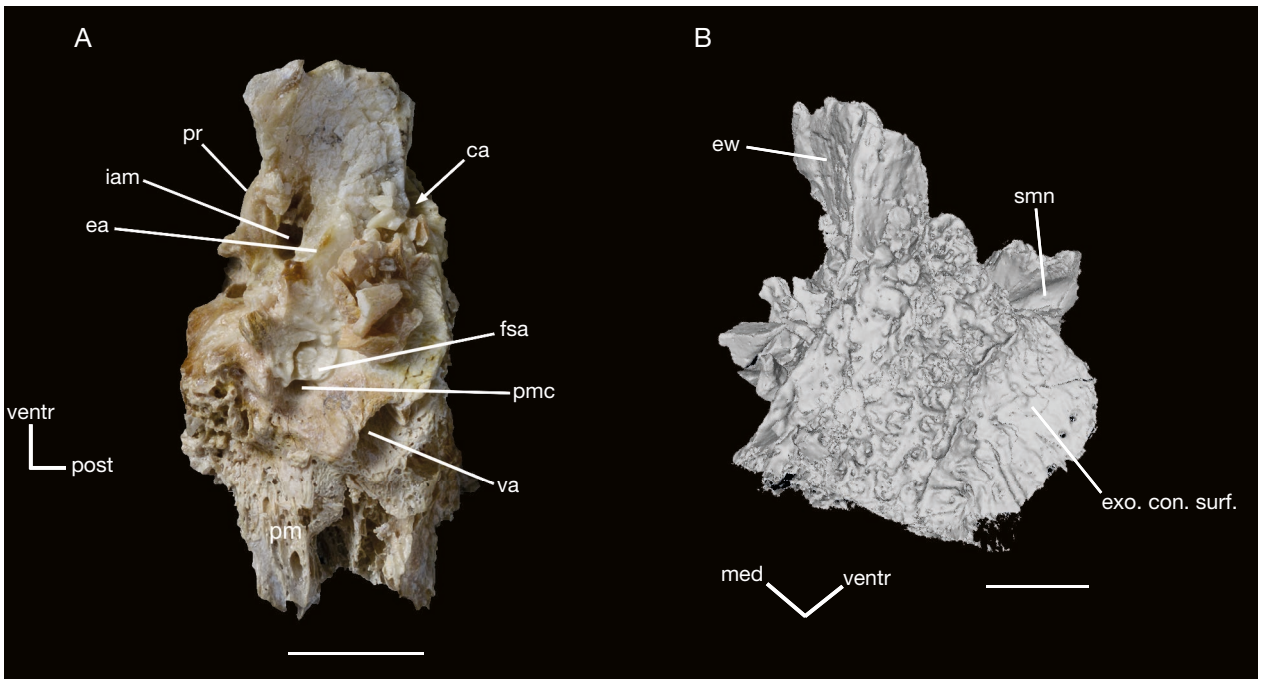

FIG. 5. — Left petrosal of *Namatherium blackcrowense* Pickford, Senut, Morales, Mein & Sanchez, 2008, referred specimen GSN BC 21'19: **A**, medial view (photograph); **B**, posteromedial view (3D digital model reconstructed from micro-CT scan). Abbreviations for petrosal morphology: **ca**, cochlear aqueduct; **ea**, eminantia arcuata; **ew**, epitympanic wing; **exo. con. surf.** (**broken**), connecting surface of the left petrosal bone with the exoccipital; **fsa**, *fossa subarcuata*; **iam**, internal auditory meatus; **pm**, mastoid part of the petrosal; **pmc**, petromastoid canal; **pr**, promontorium; **smn**, stylomastoid notch; **va**, vestibular aqueduct. Orientation axes: **med**, medial; **lat**, lateral; **post**, posterior; **ventr**, ventral. Photo by P. Loubry (CR2P, MNHN); 3D Model reconstructed by N. Poulet (CR2P, MNHN). Scale bars: 10 mm.

Its base is preserved on the right petrosal and its large dimensions suggest that the entire process had at least a moderately inflated condition. A prominent depression flaring laterally in the ventralmost preserved part of the tegmen tympani further suggests that it may have been pierced by a broad canal. In the absence of any clear indication for a transpromontorial course of the internal carotid artery, this may be identified as a canal either for the ramus superior of the stapedial artery or for the lateral head vein (prootic sinus) (see MacPhee *et al.* 2021). As in *Arsinoitherium* there is no inflated caudal tympanic process, and the postpromontorial sinus posterior to the cochlear fossula is not clearly delimited, except laterally by the *crista interfenestralis*. The stylomastoid notch for the exit of the facial nerve (VII) is very large and extends posterolaterally as a long and unclosed ossified tube (hereafter called the stylomastoid tube) in direct continuity with the facial sulcus (Fig. 4D). The stylomastoid notch opens just posterolateral to the base of the tympanohyal, the ventral extremity of which is missing. The tympanohyal is preserved as a broad process and is compressed in an oblique anterolateral-posteromedial direction. There is no distinct fallopian aqueduct, a character known in the tethytheres (Court 1992b), but the area of the hiatus Fallopii is broken on both right and left petrosals.

Only a small portion of the petrosal bone is preserved lateral to the crista parotica on the right petrosal, between the tegmen tympani anteriorly and the tympanohyal posteriorly. The epitympanic recess occurs as a large but shallow depression that excavates the posterior aspect of the tegmen tympani more than the roof of the middle ear posterior to the tegmen tympani. The recess thus faces more posteriorly than laterally or ventrally. The *fossa incudis* is located more posteriorly, on the lateral aspect of the *crista parotica*, slightly posterior to the level of the *fenestra vestibuli* and anterior to a knob-like process of unknown homology at the base of the tympanohyal. The *fossa incudis* is more distinct on the left petrosal and occurs as an ovoid fossa elongated anteroposteriorly. On both petrosals, the unidentified knob-like process located at the anterior base of the tympanohyal (see Fig. 6C) on the lateral aspect of the *crista parotica* forms the anterior wall of an unidentified foramen. This foramen represents the outlet of a canal that runs within the base of the tympanohyal, parallel to the articular surface with the squamosal bone and to the stylomastoid tube (Fig. 7). This canal opens posterolaterally (Figs. 4A, 6C. and 7, labelled "thyc", "thyc f2") and may have been connected to an internal canal within the squamosal bone. The nature and homology of this canal is unknown and to our knowledge has not been observed in other placentals.

The *pars mastoidea* is broken and incomplete. Its preserved part is highly pneumatised.

Cerebellar view. The *fossa subarcuata* is very shallow as in *Arsinoitherium*, extant tethytheres (Benoit *et al.* 2013b), and large placental species in general (Billet *et al.* 2015; Le Verger *et al.* 2024). There is a sharp ridge (*eminantia arcuata*) separating it from the internal auditory meatus. In contrast to *Arsinoitherium*, there is a fully distinct petromastoid canal in the *fossa subarcuata* (Fig. 6A). The petromastoid canal is doubled in *Namatherium*.

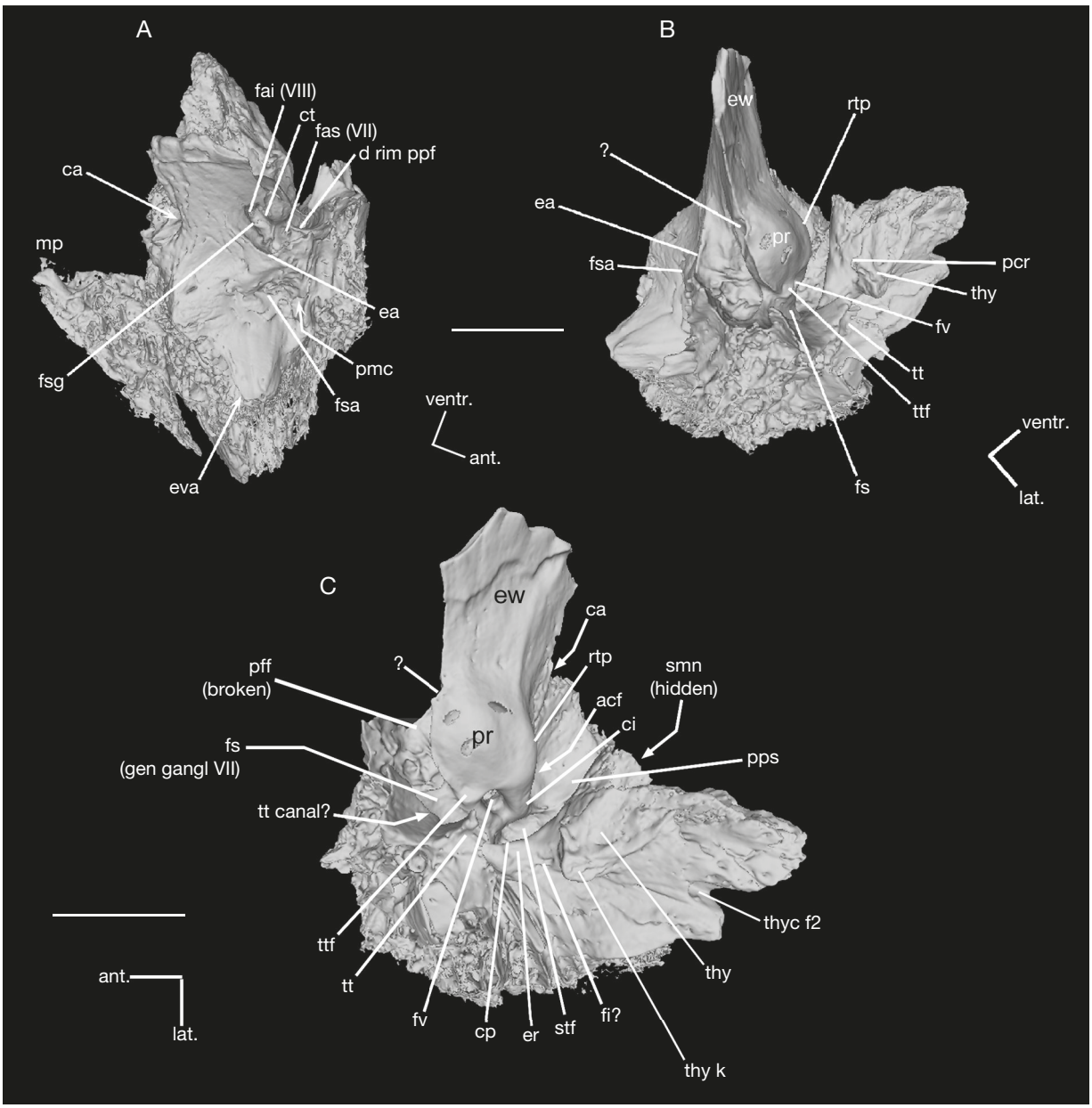

FIG. 6. — 3D digital model of the right petrosal models reconstructed from micro-CT scan (referred specimen GSN BC 21'19) of *Namatherium blackcrowense* Pickford, Senut, Morales, Mein & Sanchez, 2008: **A**, medial view; **B**, anterior view; **C**, ventral view. Abbreviations for petrosal morphology: **acf**, external aperture of the cochlear fossula; **ca**, cochlear aqueduct; **ci**, *crista interfenestralis*; **cp**, *crista parotica*; **ct**, *crista transversa*; **d rim ppf**, dorsal rim of primary facial foramen; **ea**, *eminantia arcuata*; **er**, epitympanic recess; **eva**, external aperture of the vestibular aqueduct; **ew**, epitympanic wing; **fai (VIII)**, *foramen acusticum inferius* housing the canal and cribriform tract for the cochlear nerve (see Fig. 7C); **fas**, *foramen acusticum superius*; **fi**, fossa incudis; **fs** (**gen gangl VII**), facial sulcus (geniculate ganglion of the facial nerve VII); **fsa**, *fossa subarcuata*; **fsg**, foramen singular; **fv**, *fenestra vestibuli*; **mp**, mastoid process; **pcr**, posterior crus for attachment of the ectotympanic; **pff**, primary facial foramen; **pmc**, petromastoid canal; **pps**, postpromontorial tympanic sinus; **pr**, *promontorium*; **rtp**, rostral tympanic process; **smn**, stylomastoid notch; **stf**, stapedial fossa; **thy c f2**, tympanohyal canal, posterolateral foramen; **thy k**, tympanohyal knob-like process; **thy**, tympanohyal; **ttf**, tensor tympani fossa; **tt**, tegmen tympani. Orientation axes: **ant**, anterior; **lat**, lateral; **post**, posterior; **ventr**, ventral. 3D Model reconstructed by N. Poulet (CR2P, MNHN). Scale bars: 10 mm.

The morphology of the internal auditory meatus also resembles that of *Arsinoitherium* (Court 1990): it forms a deep fossa housing the two *foramina acustica*, which are separated by a thin but distinct *crista transversa* (= *crista falciformis*). The *foramen acusticum inferius*, better preserved on the right petrosal (Fig. 6A), is very deep and oval, being elongated in the ventromedial-dorsolateral axis. It is pierced in its deepest part by small foramina forming a sieve that corresponds to the *tractus spiralis foraminosus* for the passage of fascicles of the vestibulo-cochlear nerve (nerve VIII). More laterally and dorsally, there is a small but distinct circular foramen corresponding to the *foramen singulare*. This foramen, which contained a portion of the cranial nerve VIII connected to the posterior ampulla of the vestibule (*nervus ampullaris posterior canal*), is also distinct on the reconstructed 3D Model of the labyrinth (Fig. 7D-E). The *foramen acusticum inferius* expands medially through a short and wide groove that is divided by two small median

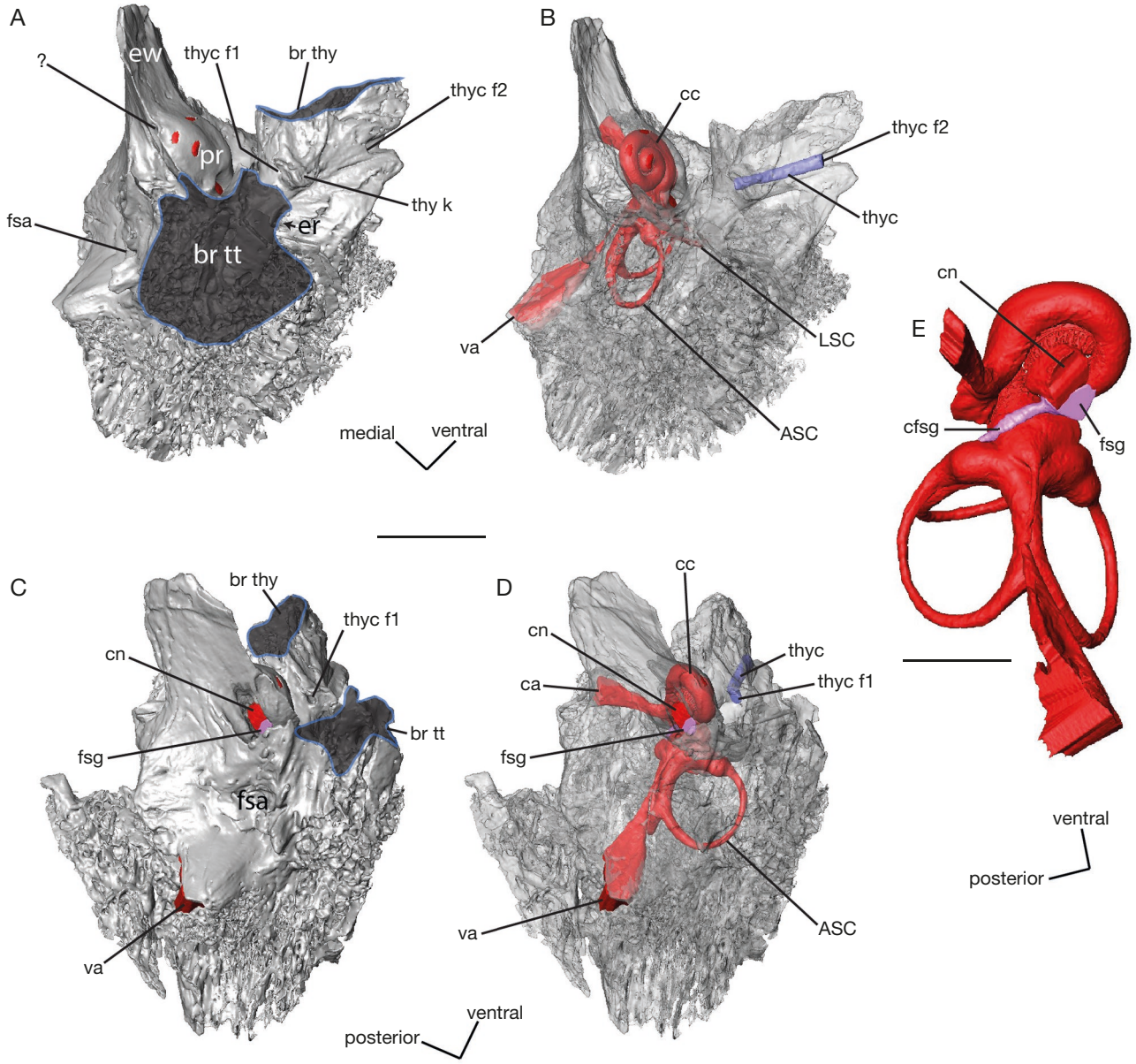

FIG. 7. — 3D digital reconstruction of the right petrosal and bony labyrinth of *Namatherium blackcrowense* Pickford, Senut, Morales & Sanchez, 2008, referred specimen GSN BC 21'19: **A**, anterior view; **B**, same as A, but with petrosal transparency leaving the bony labyrinth and stylomastoid tube visible; **C**, cerebellar view; **D**, same as C, but with petrosal transparency leaving the bony labyrinth, the foramen singulare and the stylomastoid tube visible; **E**, close-up view of the bony labyrinth and canal for the foramen singular, dorsomedial view. **Shaded areas** represent broken parts of the tegmen tympani and tympanohyal. Abbreviations: **ASC**, anterior semicircular canal; **br tt**, broken area of the tegmen tympani and primary facial foramen; **br thy**, broken area of the tympanohyal; **ca**, cochlear aqueduct; **cc**, cochlear canal; **cfsg**, canal of the foramen singulare; **cn**, canal and cribiform tract for the cochlear nerve; **er**, epitympanic recess; **ew**, epitympanic wing; **fsa**, *fossa subarcuata*; **fsg**, foramen singulare; **LSC**, lateral semicircular canal; **PSC**, posterior semicircular canal; **thyc**, indeterminate canal within the base of the tympanohyal (tympanohyal canal); **thyc f1**, tympanohyal canal, anteromedial foramen; **thyc f2**, tympanohyal canal, posterolateral foramen; **thy k**, tympanohyal knob; **?**, indeterminate sulcus (see text); **va**, vestibular aqueduct. 3D Model reconstructed by N. Poulet (CR2P, MNHN). Scale bars: A-D, 10 mm; E, 5 mm.

ridges (Fig. 6A). Antero-laterally to the *foramen acusticum inferius*, a sharp crest corresponding to the *crista transversa* separates a small (much smaller than the *foramen acusticum inferius*) subcircular fossa corresponding to a part of the *foramen acusticum superius* (Fig. 5A); it is also pierced by small foramina corresponding to a cribriform tract for the passage of the superior branch of the vestibular nerve (connecting to the superior vestibular area). The anteroventral edge of the *foramen acusticum superius* is not preserved on the two petrosals due to breakage in this region (see above), which precludes observing the outline of the canal transmitting the facial nerve (VII) towards the *cavum supracochleare*. *Arsinoitherium* departs from *Namatherium* in the absence of *crista transversa* within the internal auditory meatus (Court 1990).

On the anteromedial edge of the cerebellar surface just opposite to the promontorium, there is a sulcus running medially from the internal auditory meatus. It opens via a notch on the anteromedial edge of the promontorium (Fig. 6B, C, labelled "?"). The nature of this sulcus is unclear

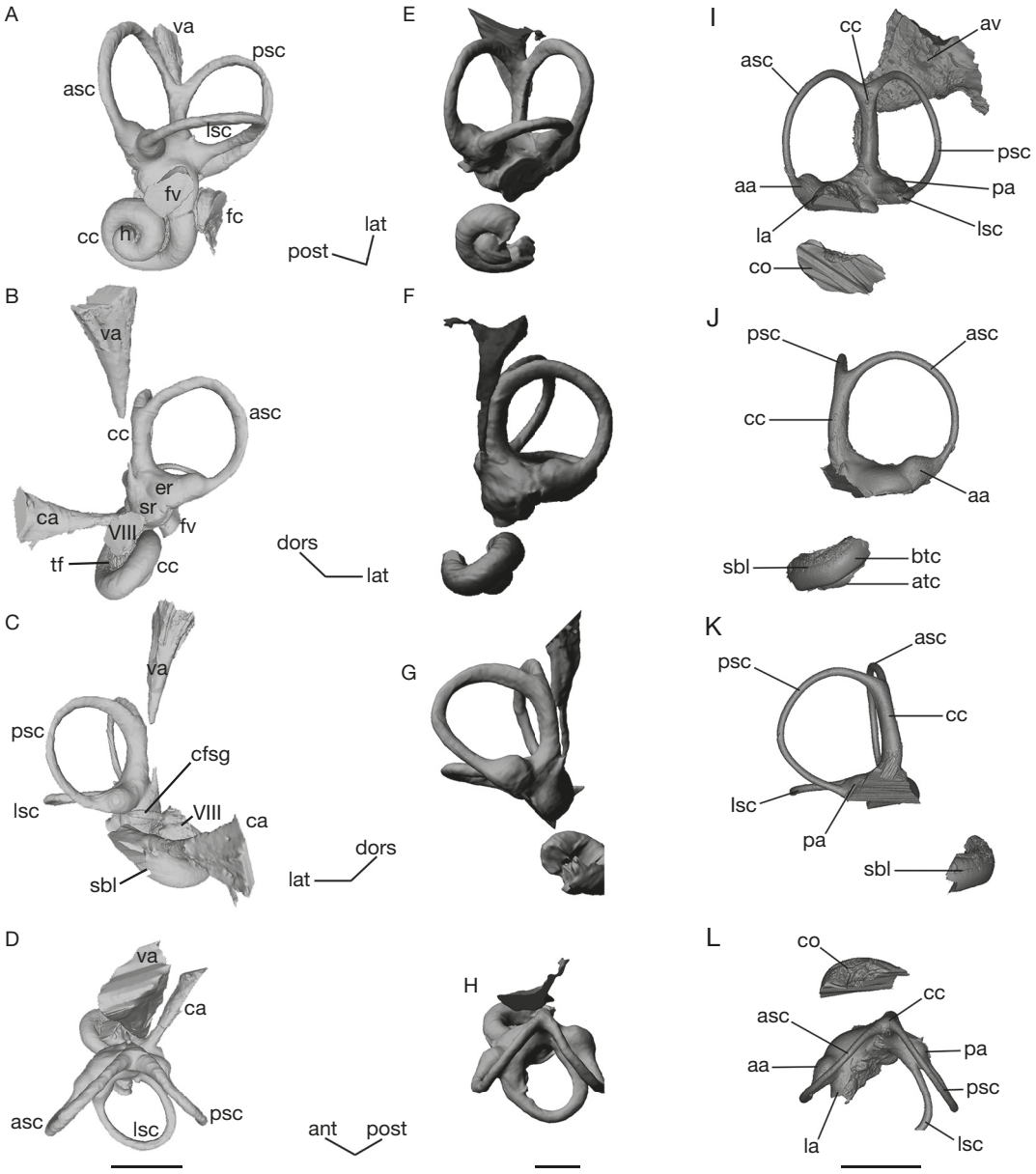

Fig. 8. — Comparison of the bony labyrinth of *Namatherium blackcrowense* Pickford, Senut, Morales & Sanchez, 2008 (**A**-**D**, left petrosal referred specimen GSN BC 21'19) with that of *Arsinoitherium zitteli* Beadnell, 1902 (**E**-**H**) and *Stylolophus major* Gheerbrant, 2021 (**I**-**L**): **A**, **E**, **I**, lateral views; **B**, **F**, **J**, anterior views; **C**, **G**, **K**, posterior views; **D**, **H**, **L**, dorsal views. **E**-**H**, from Benoit *et al.* (2013b); I-L from Gheerbrant *et al.* (2021). 3D digital models reconstructed from micro-CT scan. Abbreviations for labyrinth morphology: **aa**, anterior ampulla; **apc**, apical turn of cochlea; **asc**, anterior semicircular canal; **av**, vestibular aqueduct; **btc**, basal turn of cochlea; **cc**, *crus commune*; **ca**, cochlear aqueduct; **cfsg**, canal of *the foramen singulare* (for *nervus ampullaris posterior*); **co**, cochlear canal; **er**, elliptical recess; **fc**, *fenestra cochleae*; **fsg**, foramen singulare; **fv**, *fenestra vestibuli*; **h**, helicotrema; **la**, lateral ampulla; **lsc**, lateral semicircular canal; **pa**, posterior ampulla; **psc**, posterior semicircular canal; **sbl**, secondary bony lamina; **sr**, spherical recess; **tr**, tractus foraminus; **va**, vestibular aqueduct. Orientation axes: **ant**, anterior; **dors**, dorsal; **med**, medial; **lat**, lateral; **post**, posterior; **ventr**, ventral. **A**-**D**, 3D Model reconstructed by N. Poulet (CR2P, MNHN). Scale bars: 4 mm.

since its connections with neighbouring sulci and foramina are blurred by the extensive damage in that area. Although one might speculate that this represents the hiatus Fallopii, the latter could also have occupied a less medial position in line with the facial sulcus and *cavum supracochleare*, leaving no sulcus on the cerebellar aspect, as seen in many taxa (e.g., O'Leary 2010; Wible 2012, 2022; Benoit *et al.* 2013b; Billet *et al.* 2015; Muizon *et al.* 2015; Wible & Shelley 2020).

The vestibular aqueduct (*aquaeductus vestibuli*) opens as a large slit-like opening facing posteriorly and not visible in either dorsal or ventral views as in *Arsinoitherium*. The flattened morphology of the vestibular aqueduct was considered by Court (1990) to be derived among placentals, but this is a rather widespread feature, especially in large species. The opening of the vestibular aqueduct is far from that of the cochlear aqueduct. It is located about 22 mm postero-dorsal to the external aperture of the cochlear fossula. Their relative positions are also similar to what is known in *Arsinoitherium* (see Court 1990: fig. 2C).

Bony labyrinth (Figs 8-10)

Both the right and left bony labyrinths are well preserved in the specimen GSN BC 21'19.

Cochlea. The volume ratio of the cochlea of *Namatherium* with respect to the entire labyrinth is 44.4% which is greater by 148% than in *Arsinoitherium* (30% in Benoit *et al.* 2013b). The cochlear canal resembles that of *Arsinoitherium* in several respects. It is flat (planispiral), with a low aspect ratio of 0.5. The vestibulo-cochlear angle between the plan of the basal turn of cochlea and the axis of the *crus commune* is wide (value of its obtuse angle: 136.4-132.3°) and close to that of *Arsinoitherium* (141° in Benoit *et al.* 2013b), in contrast to a wider angle in basal eutherians (see Ekdale & Rowe 2011) and *Ocepeia* Gheerbrant & Sudre, 2001 (102° in Gheerbrant *et al.* 2020). In addition, the cochlea (basal turn) plane and LSC plane make a relatively wide angle (value of its acute angle: 52-53°) with respect to the plesiomorphic eutherian condition in which they are more parallel (e.g., Ekdale & Rowe 2011; Gheerbrant *et al.* 2020). The apex of the cochlear canal and the helicotrema remain relatively thick (not narrowed) and circular in section. The apical lacuna for the bony modiolus is large. The secondary bony lamina (*lamina secundaria*) is faint and short (Fig. 9), it does not extend beyond the first quarter of the basal turn of the cochlea (mean length = 7.4 mm; 29% of the cochlear canal length). It gradually rises from the ventral to dorsal side of the cochlear canal before disappearing (Fig. 9). The presence of a long secondary bony lamina is a plesiomorphic eutherian trait (Ekdale & Rowe 2011; Gheerbrant *et al.* 2020). The secondary bony lamina is present in *Stylolophus major* Gheerbrant, 2021 (although the cochlea is partially preserved in this species). The absence of the secondary bony lamina, also the condition in *Arsinoitherium* and elephantiforms, is related to low frequency hearing (Court 1992a; Benoit *et al.* 2023). The primary bony lamina is present and narrow (Fig. 10). The ganglion canals (spiral canal) are well defined (Fig. 10). The cochlea of *Namatherium* differs from that of *Arsinoitherium* in a few, mostly plesiomorphic traits. It has less than two turns, with about 1.7 turns (620°), in contrast to *Arsinoitherium* (720°). The cochlear whorls are well separated from each other, whereas in *Arsinoitherium* they are more coalescent.

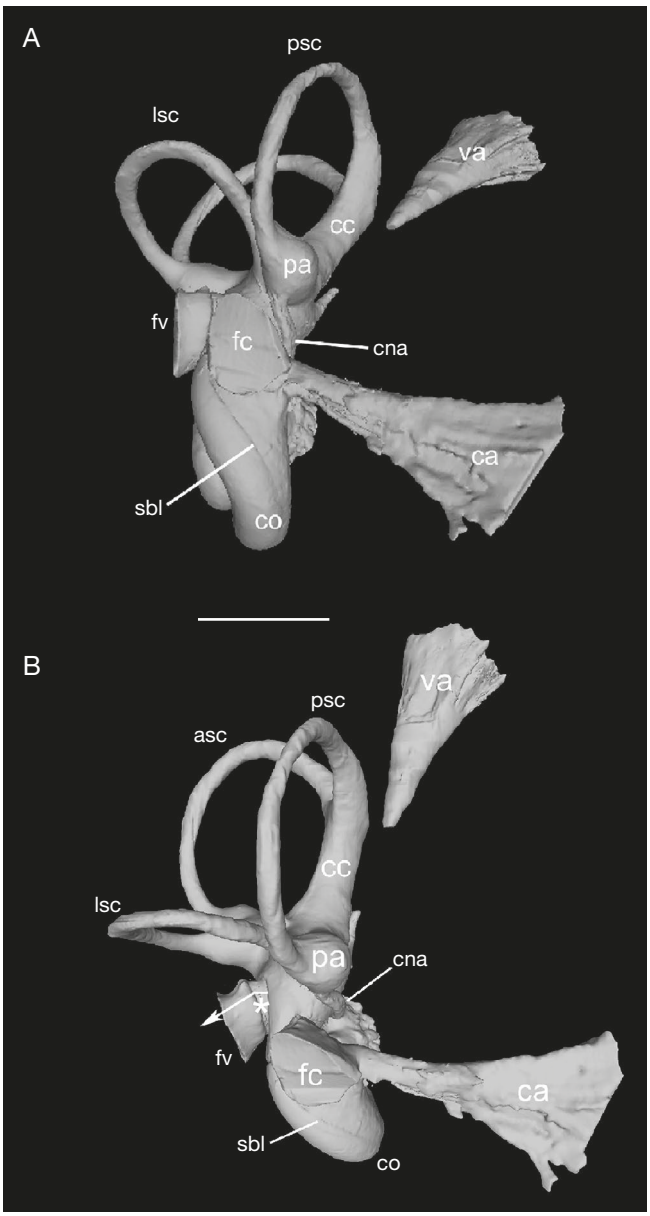

FIG. 9. — Detail of the bony labyrinth of *Namatherium blackcrowense* Pickford, Senut, Morales & Sanchez, 2008 (referred specimen GSN BC 21'19, left petrosal). 3D digital model reconstructed from micro-CT scan: **A**, view showing the short extension of the bony labyrinth, and the canal for the *nervus ampullaris posterior* (opening in the *foramen singulare*); **B**, view showing the peculiar morphology of the *fenestra vestibuli*, which is constricted at its opening on the cochlear canal (asterisk at the neck of the constriction of the fenestra) and which presents a change in its orientation (angled arrow depicting the broken axis of the fenestra opening); **A** and **B** are two subposterior views with slightly different orientations. Abbreviations: **asc**, anterior semicircular canal; **ca**, cochlear aqueduct; **cc**, *crus commune*; **cna**, canal for *nervus ampullaris posterior*; **co**, cochlear canal; **fc**, *fenestra cochleae*; **fv**, *fenestra vestibuli*; **la**, lateral ampulla; **lsc**, lateral semicircular canal; **pa**, posterior ampulla; **psc**, posterior semicircular canal; **sbl**, secondary bony lamina; **va**, vestibular aqueduct. 3D Model reconstructed by N. Poulet (CR2P, MNHN). Scale bar: 5 mm.

Vestibule. The ampullae are inflated, as in *Arsinoitherium* and *Stylolophus*. The *recessus sphericus* (spherical recess) of the saccule and the *recessus ellipticus* (elliptical recess) of the utricule are inflated and separated by a distinct groove on the vestibule. The ratio of the mean radius of curvature of the semicircular canals (SC) to the inner ear height (IEH) is 0.37 (Table 4), which indicates that the semicircular canals are well developed (see comparative data for *Ocepeia*, xenarthrans and litopterns in Billet *et al.* 2013, 2015; Gheerbrant *et al.* 2020). The semicircular canals are more or less planar and form large arcs. With a mean thickness ratio (tr) of 3.55 (for both right and left labyrinths), they are similarly stocky as in *Arsinoitherium* (tr = 3.42 in Schmitt 2016), in contrast to the thinner semicircular canals of *Stylolophus major* (mean tr = 1.46) (Fig. 8). The semicircular canals are more or less flattened with an oval cross-section. This is another remarkable trait shared with *Arsinoitherium*, especially for the anterior semicircular canal (ASC) and posterior semicircular canal (PSC) (Benoit *et al.* 2013b). It is distinct from *Stylolophus* and the generalised paenungulate condition of a more rounded SC cross-section (Gheerbrant *et al.* 2021). The planes of the semicircular canals make right angles with small variation (mean angle 86.4° for both right and left inner ears; angle variance index Log 90var = 1.25), which are thus less acute than in *Arsinoitherium* (mean angle 79°). The ASC

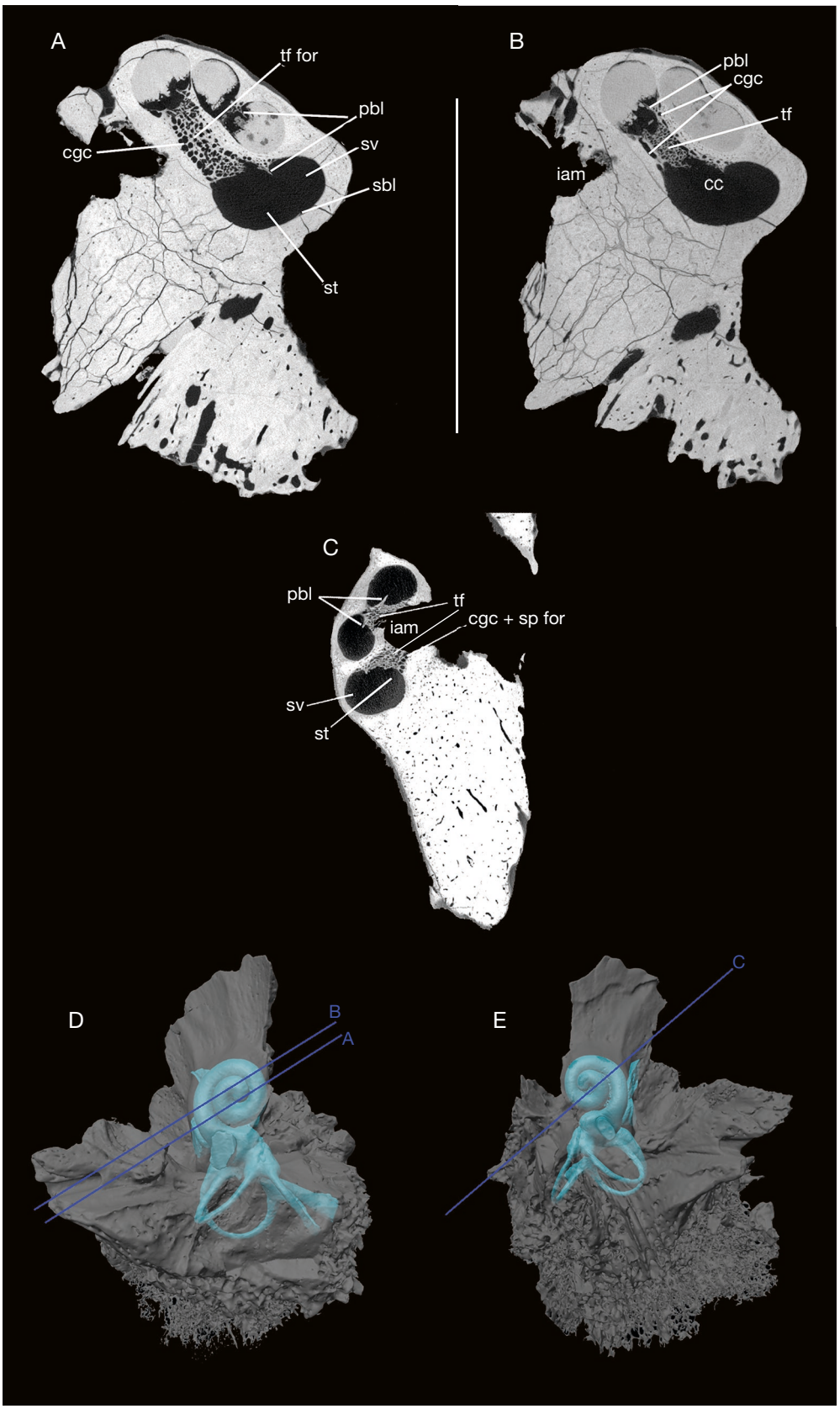

FIG. 10. — CT Scan sections of the petrosal cochlear area of *Namatherium blackcrowense* Pickford, Senut, Morales & Sanchez, 2008, referred specimen GSN BC 21'19: **A**, **B**, left petrosal; **C**, right petrosal; **D**, 3D digital model of the right petrosal showing the right labyrinth by transparency and the position of CT sections **A** and **B** (tympanic view); **E**, same as **D**, for the left petrosal, CT scan section C. Abbreviations for labyrinth morphology: **cc**, cochlear canal; **cgc**, cochlear ganglion canal; **co**, cochlea; **iam**, internal auditory meatus; **pbl**, primary bony lamina; **sbl**, secondary bony lamina; **sp for**, *tractus spiralis foraminosus*; **st**, *scala tympani*; **sv**, *scala vestibuli*; **tf for**, *tractus foraminus*. 3D Model reconstructed by N. Poulet (CR2P, MNHN). Scale bars: 5 mm.

and PSC are of similar size, the former being slightly larger and higher (Table 3). As in *Arsinoitherium*, the shape of the arc of the ASC is subcircular and that of the lateral semicircular canal (LSC) is oval (see ratios W/H in Table 3). The PSC is subcircular in contrast to that of *Arsinoitherium* (Benoit *et al.* 2013b), but similar to that of *Stylolophus*. The LSC is the smallest of the semicircular canals as in *Arsinoitherium*, although it is relatively larger and especially more elongated (more oval).

The *crus commune* reaches 76.7% of the ASC height, as in *Arsinoitherium,* but less than in *Stylolophus* (>85% of the ASC height; Gheerbrant *et al.* 2021) (Fig. 8). It has a thickness ratio (tr) of 24.53 (mean of the right and left labyrinths), which indicates a stockier *crus commune* than in *Stylolophus major* (tr = 13.7 in Benoit *et al.* 2023) and also in *Arsinoitherium* (tr = 14.55 in Schmitt 2016). *Namatherium* lacks a secondary common crus, like *Arsinoitherium.* However, the morphology of the posterior branch of the LSC is in an intermediate state between *Arsinoitherium* and *Stylolophus*: it is partially coalescent with the posterior ampulla but less fused than in *Stylolophus*. In lateral view, the *crus commune* is slightly inclined posteriorly with respect to the LSC, in a similar degree to *Arsinoitherium*. The *fenestra vestibuli* opens well ventral to the lateral ampulla, and in an orthogonal plane with respect to the cochlear fenestra. The *fenestra vestibuli* is oval and large, and only slightly smaller than the *fenestra cochleae*.

The cochlear aqueduct (*aquaeductus cochleae*) is long (8.35 mm in the right petrosal), which implies a major size difference between the inner ear and the petrosal bone that contains it (Fig. 7) (Billet *et al.* 2015). It extends medially and posteriorly, in a plane parallel to that of the LSC, and it flares gradually. Its section is anteroposteriorly - mediolaterally compressed. The cochlear aqueduct is partly coalescent at its entry on the cochlear canal with the *fenestra cochleae* and with the proximal part of the cochlear fossula (Figs 8; 9). This is reminiscent of the morphology seen in *Prorastomus* (Benoit *et al.* 2013a). The specialised distinctive condition of a single perilymphatic foramen seen in *Arsinoitherium* is only known in modern tethytherians such as extant sirenians and proboscideans, where it evolved as homoplasies (Court & Jaeger 1991; Court 1994; Savage *et al.* 1994; Gheerbrant *et al.* 2005; Benoit *et al.* 2013a, b; Gheerbrant *et al.* 2021). The vestibular aqueduct (*aquaeductus vestibuli,* endolymphatic canal) is much thinner than in *Arsinoitherium*, but its general shape is similar. It originates from a bulged pyramid-like area of the vestibule, ventromedial to the *crus commune*, that is quite distinctive. It is significantly longer (15.7 mm in the right petrosal) than the cochlear aqueduct. It extends as a very thin canal parallel to the *crus commune*, and it enlarges above the *crus commune* into a fan-like shape. It extends dorsally well beyond the dorsal tip of the common crus. There is a thin but distinct canal for the *nervus ampullaris posterior* (Figs 7; 8, labelled "cfsg") linking the posterior ampulla to the cochlear nerve via the *foramen singulare*. This canal leading to the foramen singulare is tightly appressed to the vestibule. Ventral to the anterior ampulla, in between the utricule and saccule, there is a small bulge (more distinct on the left inner ear) that might correspond to the foramen for the superior vestibule area.

TABLE 4. — Radius of curvature of the semicircular canals of *Namatherium blackcrowense* Pickford, Senut, Morales & Sanchez, 2008. Radius of curvature calculated following the Spoor-Zonneveld equation (Spoor & Zonneveld 1998): R = ((H+W)/2) × 0.5, with H = height and W = width of the canals.

Radius of curvature (mm)	ASC	PSC	LSC	Mean all SC
Left labyrinth	3.69	3.45	3.01	3.38
Right labyrinth	3.67	3.47	2.91	3.35
Mean left and right	3.68	3.46	2.96	3.37

TABLE 5. — Body mass (**BM**) estimates of *Namatherium blackcrowense* Pickford, Senut, Morales & Sanchez, 2008 in kilograms. Predictive allometric equations from Damuth & MacFadden (1990a, b) based on dental measurements: 1) for all ungulates; and 2) for non-selenodont ungulates. Predictive equation from intercondylar width after Engelman (2022). Best estimates are **in bold**; our best estimate of the body mass of *Namatherium blackcrowense* is around 350 kg, with a possible range of 300-450 kg; this corresponds to the estimate obtained from interoccipital condyle width (measured on specimen GSN BC 21'19), and from the size of the first molar employing dental measurements.

Reference measurements	**Estimated BM**	
Occipital condyle width (OCW = 92.79 mm)	**345 kg**	
Tooth size (mean right and left)	**1) All ungulates pred. equation**	**2) Non selenodont pred. equation**
M1-3 length (103.33 mm)	592 kg	503 kg
M1 length (26.71 mm)	**416 kg**	**353 kg**
M2 length (37.04 mm)	725 kg	541 kg
M3 length (39.74 mm)	608 kg	497 kg
M1 area (767.93 mm²)	**454 kg**	**309 kg**
M2 area (1359.62 mm²)	737 kg	494 kg
M3 area (1607.89 mm²)	940 kg	644 kg

BODY MASS ESTIMATE OF *NAMATHERIUM BLACKCROWENSE* (TABLE 5)

Recent study by Engelman (2022) showed that one of the most reliable currently used estimates of body mass in mammals from skeletal measurements is that based on the occipital condylar width (OCW) which is fortunately preserved in the new specimen of *Namatherium blackcrowense* (GSN BC 21'19) described herein. We also estimated the body mass of *N. blackcrowense* on the basis of dental measurements. The estimate of the body mass of *N. blackcrowense* from occipital condylar width (345 kg) is in the lower range of estimates based on tooth size, and is closer to estimates based on upper first molar size (309-454 kg). We provide estimates of *N. blackcrowense* body mass from tooth size using the predictive equations for all ungulates and for non-selenodont ungulates (Damuth & MacFadden 1990a, 1990b), the latter being most appropriate for the lophodont-like *Namatherium*. Accordingly, our best estimate of the body mass of *Namatherium blackcrowense* is close to 350 kg, with a wide possible range between 300 kg and 450 kg (Table 5).

In Figure 12 we plotted the size of the semicircular canals (as estimated by the radii of curvature) *versus* the body mass of *Namatherium blackcrowense,* in comparison to other afrotherians and various placentals. It shows that *Namatherium* has semicircular canals of small to medium size with respect to its body size. Similarly, the embrithopods *Stylolophus* and *Arsinoitherium* have medium-sized semicircular canals for their respective body mass (see table of measurements in Appendix 4).

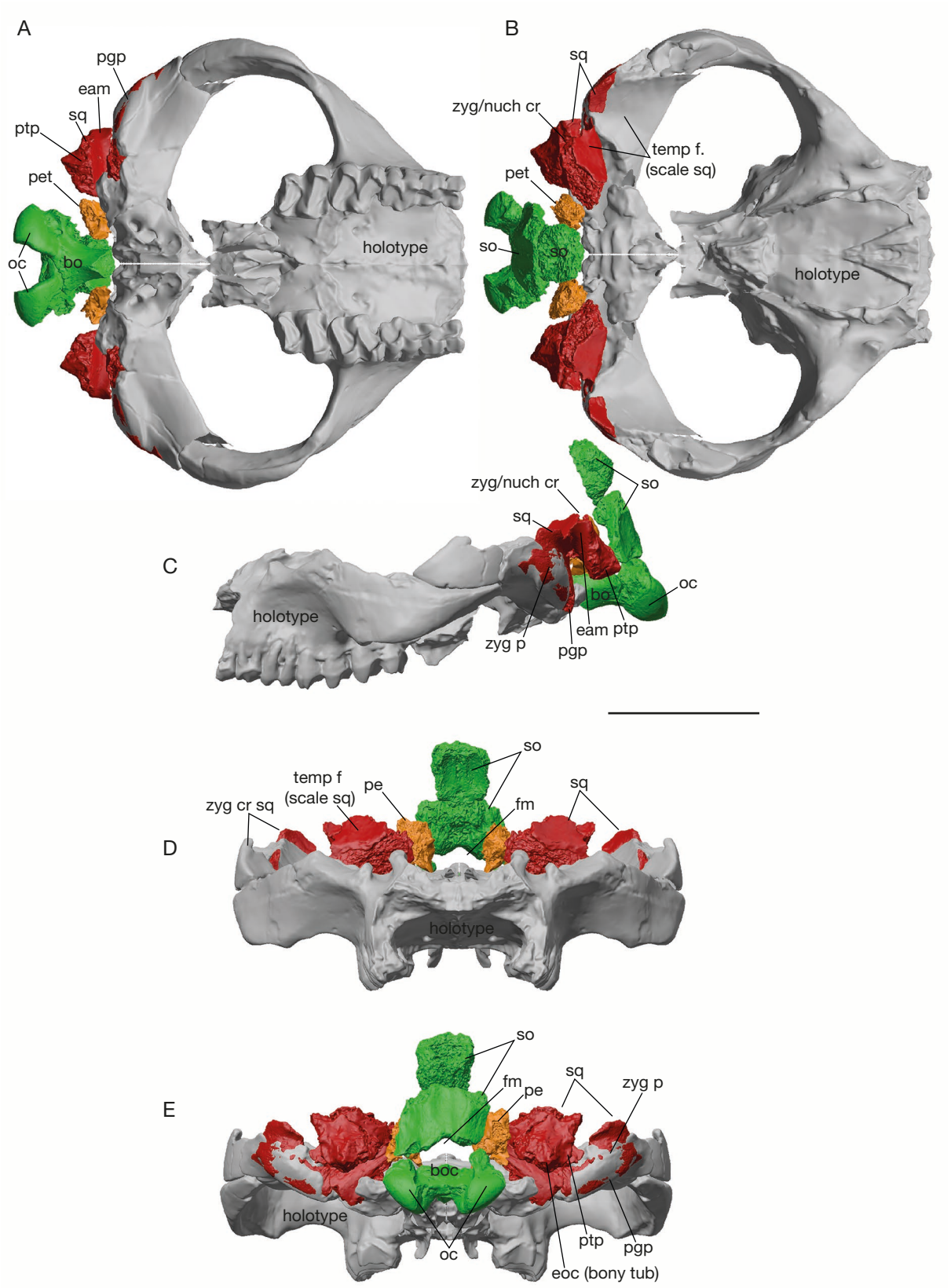

FIG. 11. — Composite reconstruction of the skull of *Namatherium blackcrowense* Pickford, Senut, Morales & Sanchez, 2008 based of the new specimen GSN BC 21'19 and the holotype GSN BC 13'08: **A**-**E**, ventral (**A**), dorsal (**B**), lateral (**C**), anterior (**D**) and posterior (**E**) views. The reconstruction of the posterior and basicranial parts of the skull was made by assemblage of the 3D digital models of the broken bones of GSN BC 21'19 that were obtained from surface-scanning. The reconstruction of the anterior and median parts of the skull is based on a restored model of the holotype GSN BC 13'08 where distorted and missing parts were corrected and completed as far as possible by mirror-imaging of the best preserved bones. See also Appendix 3. Abbreviations: **boc**, basioccipital; **boc pr**, basioccipital process for attachment of the posttympanic process of squamosal; **eam**, external auditory meatus; **eoc** (bony tub), exoccipital bony tuberosity; **fm**, foramen magnum; **pet**, petrosal; **oc**, occipital condyle; **pgp**, postglenoid process; **ptp**, posttympanic process; **so**, supraoccipital; **sq**, squamosal; **temp f**, temporal fossa (scale of the squamosal); **zyg/nuch cr**, zygomatic and nuchal crest; **zyg p**, zygomatic process. 3D Model reconstructed by F. Goussard (CR2P, MNHN). Scale bar: 10 cm.

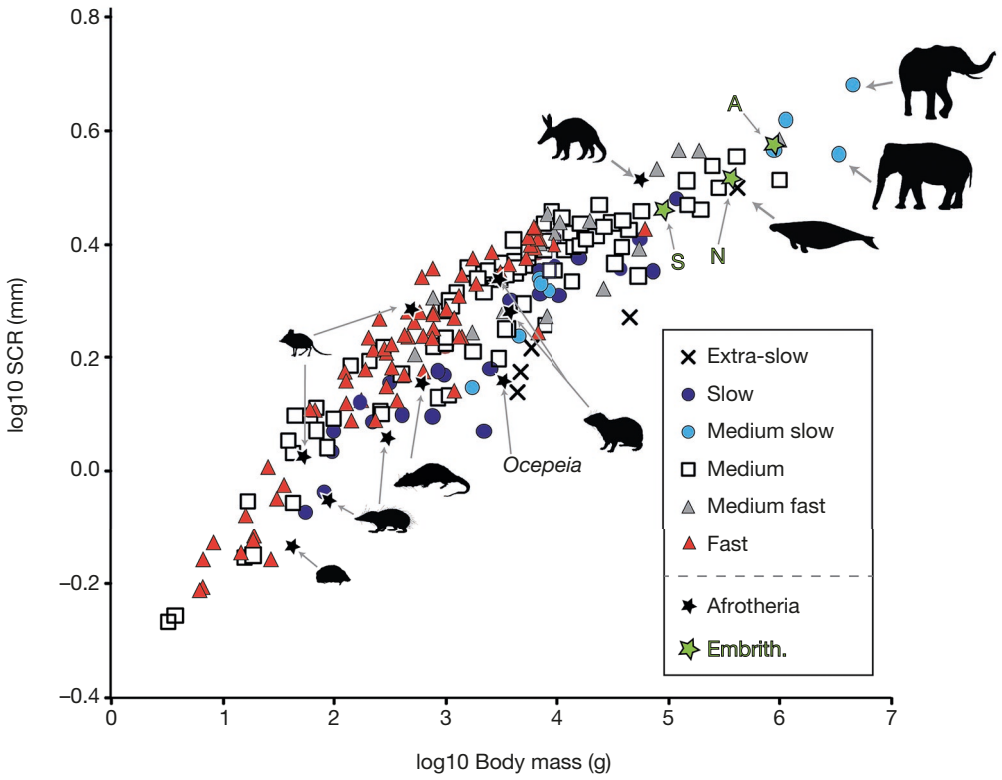

FIG. 12. — Graphical relationship between the size of the semicircular canals (**SCR**, radius of curvature) vs body mass (**BM**), with the indication of agility estimates in *Namatherium* Pickford, Senut, Morales, Mein & Sanchez, 2008 and various mammals. Measurements of taxa other than *Namatherium* are from Spoor *et al.* (2007) and Gheerbrant *et al.* (2020). This diagram shows that *Namatherium* has relatively small to medium-sized semicircular canals with respect to other mammals of the same body mass as in other afrotherians measured. See Appendix 4 for measurements of the embrithopods.

COMPARISONS AND DISCUSSION

The new cranial specimen GSN BC 21'19 from Black Crow described above, particularly the squamosal and petrosal, is herein compared with various taxa but especially with the sympatric species *Namatherium blackcrowense*, the relationship of which is suggested by several shared characters, which are discussed below. Morphological features of the new Black Crow specimen GSN BC 21'19 are further analysed at a wider scale, together with the cranial characters described by Pickford *et al.* (2008b) in the holotype of *Namatherium blackcrowense,* especially in order to clarify the phylogenetic position of the Black Crow species within African and North Tethyan embrithopods.

Close specific affinity of the specimen GSN BC 21'19 with *Namatherium blackcrowense* is supported primarily by the similar, if not identical, size and the overall robust cranial morphology. In addition, the construction of the zygomatic process of the squamosal perfectly matches in the two specimens (see Fig. 11). In particular, the glenoid fossa is shallow and flat, and the postglenoid process preserved in specimen GSN BC 21'19 is low above the glenoid fossa and transversally elongated, exactly as in the holotype of *Namatherium blackcrowense*. Another remarkable resemblance is the laterally widely divergent zygomatic process. These shared traits unambiguously support the conspecific relationship between GSN BC 21'19 and the holotype of *Namatherium blackcrowense*. It is noteworthy that the new specimen GSN BC 21'19 preserves the basicranium and the posterior part of the skull that is lacking in the holotype. In fact, the two cranial specimens complement each other so well anatomically (for example GSN BC 21'19 includes the right squamosal, absent in the holotype), as well as being identical in size, that one could postulate whether they belong to the skull of the same individual. However, the two specimens were found in situ at localities about 270 metres apart (Fig. 1) which renders the scenario unlikely.

There are several additional specialised features shared with *Arsinoitherium* which confirm the embrithopod affinities of GSN BC 21'19, given that *Namatherium blackcrowense* is the only embrithopod known in the Black Crow site. The squamosal bears a very deep external auditory meatus that is positioned high on the skull (at orbit level), a stout and large zygomatic process, and a weak paroccipital process. The foramen magnum is enclosed dorsally by the exoccipitals. On the petrosal, the *fossa subarcuata* is absent (shallow), the medial caudal tympanic process is weak (uninflated) to absent, there is a deep common fossa for the internal auditory meatus, and the *crista transversa* is thin between the *foramina acusticum superius* and *inferius*. Some of these features such as the absence of the *fossa subarcuata* and the deep common fossa for the internal auditory meatus might be related to the large size of *Namatherium* and *Arsinoitherium* and the negative allometry of the labyrinth with the surrounding petrosal (Billet *et al.* 2015). Remarkable shared features of the bony labyrinth include thick and flattened semicircular

canals, weak and short secondary bony lamina in line with its complete (derived) absence in *Arsinoitherium*, thick *crus commune*, secondary *crus commune* absent, the cochlear aqueduct partially coalescent with the *fenestra cochleae* and the cochlear fossula which is reminiscent of the unique perilymphatic duct of *Arsinoitherium*, the wide vestibulo-cochlear angle (derived among afrotherians and paenungulates; Schmitt 2016; Benoit *et al.* 2023), the oval outline of the lateral semicircular canal, and the flat (planispiral) cochlear canal. These morphological affinities provide further arguments for the formal referral of specimen GSN BC 21'19 to the species *Namatherium blackcrowense.* They also support the Arsinoitheriidae familial referral of *Namatherium.* This agrees with several other traits of *Namatherium* shared with *Arsinoitherium* that have already been reported on the holotype by Pickford *et al.* (2008a), including the likely presence of nasal horns.

However, *Namatherium* departs from *Arsinoitherium* in many features that are less specialised. Most of the differences were identified by Pickford *et al.* (2008b) based on the holotype. Comparison of the new specimen GSN BC 21'19 allows the identification of additional distinctive traits in *Namatherium*. The external auditory meatus is more widely open (postglenoid process more recurved posteriorly and the posttympanic process more shifted anteriorly in *Arsinoitherium*). The hypoglossal (condylar) foramen is present and large, while it is fused with the jugular fossa in *Arsinoitherium*. The postglenoid foramen is present in contrast to *Arsinoitherium* (Court 1992b). The occipital condyles are less pedunculate. The *fenestra vestibuli* is oval (round with lower stapedial ratio in *Arsinoitherium*). The cochlear aqueduct is still separated from the *fenestra cochleae* whereas in *Arsinoitherium* it is fused with the *fenestra cochleae* as a single perilymphatic foramen. The cochlear canal is shorter (<2 turns), and its whorls are more separate. The semicircular canals are thinner. The *crus commune* is longer. The posterior semicircular canal is subcircular, unlike its oval outline in *Arsinoitherium*. The lateral semicircular canal is shorter and more oval. The petromastoid canal is present. The large stylomastoid tube seen in *Namatherium* is an unusual feature in paenungulates and afrotherians that might be autapomorphic. The canal piercing the base of the tympanohyal (tympanohyal canal) is also a remarkable feature of *Namatherium* that has not been described in *Arsinoitherium*.

PHYLOGENETIC ANALYSIS (Fig. 13)

We investigated the relationships of *Namatherium* within the Embrithopoda based on the morphology of both the holotype and the new specimen GSN BC 21'19 described here. For this, we employed a cladistic analysis of the matrix of Gheerbrant (2023) with some modifications (see section Material and Methods), especially with the addition of new features of the petrosal described in *Namatherium* (i.e., inner ear characters 191, 193, 199, 200). The standard analysis with TNT 1.6 provides 63 MPTs (length = 1035 steps, CI = 32.9; RI = 60.1) that are well resolved for the Paenungulata and have a topology (Fig. 13) almost identical to that found by Gheerbrant (2023). The most relevant and new result concerns the relationship of *Namatherium* that is recovered in all MPTs as the sister group to *Arsinoitherium,* albeit with low Bremer support (BM =1; Bootstrap = 61). In other words, the cladistic analysis supports the Arsinoitheriidae familial position of *Namatherium*. The clade Arsinoitheriidae including *Namatherium* and *Arsinoitherium* is supported by three exclusive synapomorphies: molar pseudohypocone (metaconular hypocone) secondarily reduced and incorporated into the lingual cingulum (character 122-2; RI = 100); molar protocone very small (character 123-2; RI = 100), and deep palate between right and left premolars (character 143-2; RI = 100). Another important exclusive character, although ambiguous, is recovered in the DELTRAN optimisation: the thick semicircular canals (character 199-1; RI = 100). This character is actually homoplastic in the tethytheres as it also evolved in modern proboscideans of the Elephantiformes clade which are not included in this analysis. In the ACCTRAN optimisation the presence of thick semicircular canals is a synapomorphy of both the arsinoitheriids and the palaeoamasiids; however, we favour the alternative hypothesis of an exclusive synapormophy (DELTRAN optimisation) of *Namatherium* and *Arsinoitherium* given their overall more advanced state of evolution (incl. dentition and petrosal features) with respect to both the palaeoamasiids and *Stylolophus*. Several unambiguous but homoplastic characters additionally support the close relationships of *Arsinoitherium* and *Namatherium*. The two most important ones (i.e., with RI = or > 70) are the P^4 with one loph (character 90-1, RI = 71) and the M^3 with 3 lingual roots (character 131-3, RI = 88). Several other interesting, although more homoplastic, characters are recovered as synapomorphies of *Arsinoitherium* and *Namatherium* in DELTRAN optimisation: the flattened semicircular canals (198-1, RI= 50), the *fossa subarcuata* absent (191-2, RI = 50), the secondary bony lamina reduced (194-1, RI = 33) and the uninflated medial caudal tympanic process (192-0, RI = 50). Among these traits, however, it should be noted that the absence of a *fossa subarcuata* is a character likely linked to large size (Billet *et al.* 2015), which is indeed a feature shared by *Namatherium* and *Arsinoitherium*. As for the thick semicircular canals, in the alternative ACCTRAN optimisation these characters are more inclusive synapomorphies of both the arsinoitheriids and the palaeoamasiids, or even of all embrithopods (characters 192-0, 193-1). However, they are optimised in the palaeoamasiids by default of knowledge in this poorly known family. These characters are instead here considered to be more likely exclusive arsinoitheriid synapomorphies, as in the case of the thick semicircular canals. There are some other remarkable shared traits of *Arsinoitherium* and *Namatherium*, but which are either not coded or decomposed into several detailed traits and states in the analysed matrix. They include the likely presence of nasal horns in *Namatherium blackcrowense* (Pickford *et al.* 2008a), and the pseudolophodont molar pattern. The pseudolophodonty of the Arsinoitheriidae, which corresponds to a molar morphology simplified to two large transverse lophs formed by the anterior crest of the paracone and metacone,

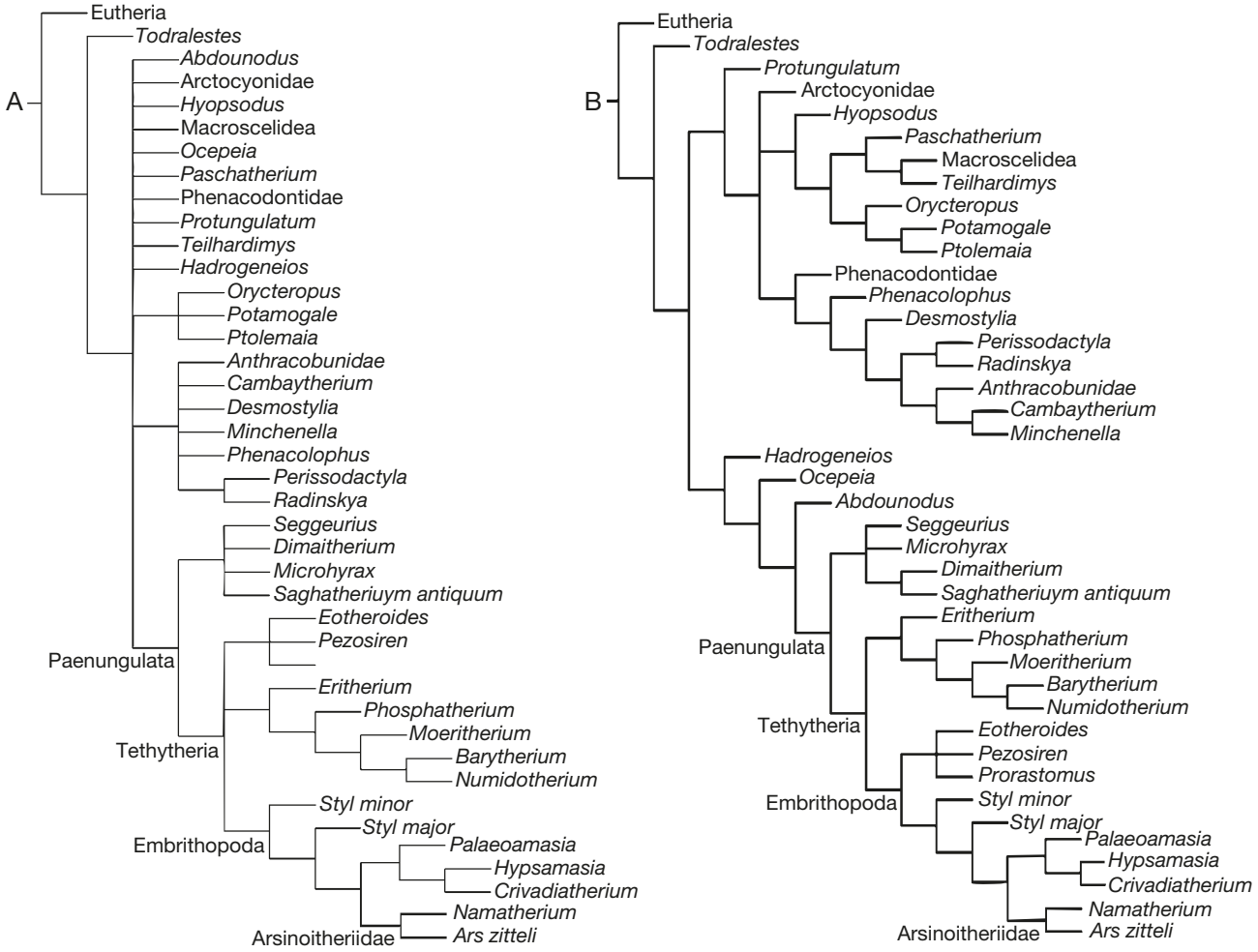

FIG. 13. — Relationships of *Namatherium* Pickford, Senut, Morales, Mein & Sanchez, 2008 and the embrithopods resulting from cladistic analysis with TNT1.6. Strict consensus tree (**A**) and Majority Rule Tree (**B**) of 63 MPTs obtained from the standard analysis. Retention index RI: 60.1; consistency Index CI: 32.9. Tree length: 1036 steps. Details of the matrix and cladistic analysis are provided in the Material and Methods section. The analysed matrix is provided in Appendix 2.

is a combination of the following characters states in our matrix: 122-2, pseudohypocone (= metaconular hypocone) absent; 108-2, postparacrista absent; and 109-3 postmetacrista residual.

The close relationship of *Namatherium* to *Arsinoitherium* is also consistent with the presence in *Namatherium* of some features that are in an intermediate state between the plesiomorphic condition of embrithopods (and paenungulates) and the most derived condition of *Arsinoitherium.* This includes especially the petrosal features 190 and 196. In *Namatherium*, the partly coalescent cochlear aqueduct with the *fenestra cochleae* and cochlear fossula (state 190-1; homoplastic within tethytheres) is a derived trait with respect to the more distant position of the cochlear aqueduct from the *fenestra cochleae* (state 190-0) that is a generalised condition known in basal eutherians such as zhelestids (Ekdale & Rowe 2011), and in paenungulates such as *Ocepeia*, *Seggeurius*, *Procavia* Storr, 1780, *Phosphatherium* Gheerbrant, Sudre & Cappetta, 1996, and probably even *Stylolophus* (Gheerbrant *et al.* 2021). The partly coalescent cochlear aqueduct with the *fenestra cochleae* is actually an intermediate state (state 190-1) between the primitive paenungulate condition, with a more separated cochlear aqueduct and *fenestra cochleae* (state 190-0), and the specialised morphology of *Arsinoitherium* in which the cochlear aqueduct and the *fenestra cochleae* are merged into a single perilymphatic foramen (state 190-2). However, it should be noted that the condition seen in *Namatherium* is also known in some other early, non-paenungulate, placental taxa such as *Didelphodus* Cope, 1882 and *Protungulatum* Sloan & Van Valen, 1965 (GB pers. obs.). Whatever the case, *Namatherium* yields additional evidence of the homoplastic evolution of the perilymphatic foramen in the tethytheres (Court & Jaeger 1991; Court 1994; Savage *et al.* 1994; Gheerbrant *et al.* 2005; Benoit *et al.* 2013a, b; Gheerbrant *et al.* 2021). The morphology of the posterior branch of the lateral semicircular canal (character 196) in *Namatherium* is also in an intermediate state within the embrithopods: it is tightly appressed against and partially fused to the posterior ampulla (state 196-1), but less fused than in *Stylolophus* (state 196-0) and more so than in *Arsinoitherium* which completely lacks a secondary common crus (state 196-2).

The clade including *Arsinoitherium* and *Namatherium*, i.e. the family Arsinoitheriidae, is sister group to the Palaeoamasiidae in our resulting MPTs. The relationships of *Stylolophus minor* Gheerbrant, 2018 and *S. major* Gheerbrant, 2021 from the early Eocene of Morocco as successive stem groups to both the Arsinoitheriidae and the Palaeoamasiidae, i.e. as stem embrithopods, is consistent with the hypothesis of an African origin for the Embrithopoda and the northward trans-Tethyan dispersal of a *Stylolophus*-like stem palaeoamasiid (Gheerbrant *et al.* 2018). However, we should note that the palaeoamasiid clade combining known north Tethyan embrithopods remains supported by only a few homoplastic features (and low Bremer support and Bootstrap), several of which are optimised due to a lack of knowledge (e.g.; unknown upper dentition of *Crivadiatherium* Radulesco, Iliesco & Iliesco, 1976). New fossil discoveries of the poorly-known family Palaeoamasiidae would shed much light on embrithopod relationships.

CONCLUSION

The new material from the Eocene of the Black Crow site (Namibia) described here belongs to the African embrithopod species *Namatherium blackcrowense*, previously known by a single partial skull. The specimen GSN BC 21'19, which corresponds to the broken posterior part of a skull, significantly completes the holotype and allows us to reconstruct much of the skull of *N. blackcrowense* (Fig. 11), with the exception of the mandible which is still unknown.

The specimen GSN BC 21'19, together with the holotype of *N. blackcrowense*, provides important new morphological and phylogenetic data on advanced African embrithopods. Our comparisons and cladistic analysis support a close sister-group relationship between *Namatherium* and *Arsinoitherium* and their appurtenance to the same family, the Arsinoitheriidae, as suggested by Pickford *et al.* (2008b). This relationship is further supported by some remarkable shared specialised traits of the petrosal and inner ear seen on GSN BC 21'19 such as the thick and flattened semicircular canals, the subarcuate fossa absent, the reduced (short) secondary bony lamina, and the cochlear aqueduct partially fused with *fenestra cochleae* and cochlear fossula in *Namatherium* that foreshadows the unique perilymphatic foramen of *Arsinoitherium*. The reduced secondary bony lamina indicates an inner ear specialised for low-frequency hearing in both *Namatherium* and *Arsinoitherium*. These basicranial characters add to the arsinoitheriid synapomorphies displayed by the holotype of *Namatherium* such as the pseudolophodont dentition and the development of hollow nasal horns.

The relationship of *Namatherium* highlights an old endemic evolution of the Arsinoitheriidae in Africa, since the middle Eocene, with important fossil gaps in the middle and late Eocene. The morphological information yielded by *Namatherium* helps to reconstruct the ancestral morphotype of the family Arsinoitheriidae. It further emphasises the highly autapomorphic condition of *Arsinoitherium zitteli* Beadnell, 1902. This implies a significant evolution (divergence) of the *Arsinoitherium* lineage with respect to *Namatherium* which remains undocumented between the Lutetian (*c.* 47.8 Ma) and the Priabonian (*c.* 37.8 Ma).

Our phylogenetic analysis supports the conclusion that the African Arsinoitheriidae and the North Tethyan Palaeoamasiidae share an African common ancestor that is sister-group to *Stylolophus major* and *S. minor* from the Early Eocene. After the trans-Tethyan dispersal from Africa of a *Stylolophus*-like stem palaeoamasiid (Gheerbrant *et al.* 2018, 2021), the two families Arsinoitheriidae and Palaeoamasiidae evolved separately on the two sides of the Tethys during the middle-late Eocene and the Oligocene. As far as we know, palaeoamasiids remained conservative, at least dentally, throughout their evolution in the insular palaeogeographic context of Balkanatolia (Licht *et al.* 2022). In contrast, the Arsinoitheriidae evolution was characterised by gigantism, highly specialised teeth and striking autapomorphic traits such as huge nasal horns and also by some unexpected reversals. The remarkable reversals of *Arsinoitherium* concern mostly tethytherian morphotypic traits (see Gheerbrant *et al.* 2021) such as the narrow zygomatic arches, the posterior position of the orbits, the ventral rim of the orbits comprising the jugal instead of the maxilla, the weak lateral zygomatic process of the squamosal and a subvertical I/1 (i.e., lower central incisor not procumbent as in *Stylolophus*). These morphological reversals remain to be explained functionally and adaptively in the Eocene African palaeoenvironmental context. An important palaeoclimatic event at this time was the Middle Eocene Thermal Maximum (Scotese *et al.* 2021), at *c.* 43.5 Ma. It may have had significant impact on the evolution and composition of the African Eocene flora, and consequently on the evolution of the African megaherbivorous mammals, especially the highly specialised arsinoitheriids. Last but not least, *Namatherium* shows that arsinoitheriids were widespread, ranging from north to south (see Fig. 1), over the African cradle.

Acknowledgements
Thanks to the Geological Survey of Namibia, the Ministry of Mines and Energy, the Ministry of Environment and Tourism, the Namibian National Heritage Council, The National Commission for Research, Science and Technology, and Namdeb for encouraging the long term research project in the Sperrgebiet. Thanks to the French Embassy in Namibia for local support. Funding was provided by the Sorbonne Université (Muséum national d'Histoire naturelle, Paris, UMR 7207 and CR2P (CNRS, MNHN), the Collège de France and Namdeb. The specimen GSN BC 21'19 was CT scanned at the « AST-RX, plateau d'accès scientifique à la tomographie à rayons X du MNHN, UMS 2700 outils et méthodes de la systématique intégrative CNRS -MNHN, PARIS.» We thank especially M. Bellato (MNHN) for her help with acquisition of the CT scans. Thanks to P. Loubry (CR2P) for the excellent photographs of the material described here. Thanks also to N. Poulet (CR2P) and

F. Goussard (CR2P) for their helpful assistance with 3D digital reconstructions and imaging based on CT scans, and also for measurements on CT scan images and 3D digital models. N. Poulet helped us with the 3D modelling of the petrosals and labyrinths, and F. Goussard with the modelling and reconstruction of the skull of *Namatherium* (Fig. 11; Appendix 3). We also thank R. Vacant (CR2P) for the acid preparation of the new *Namatherium* specimen, in particular for the careful separation of the two petrosal bones from the limestone matrix. We thank the two referees and the editor for their comments and corrections of the manuscript.

REFERENCES

ANDREWS C. W. 1906. — *A Descriptive Catalogue of the Tertiary Vertebrata of the Fayûm, Egypt. Based on the Collection of the Egyptian Government in the Geological Museum, Cairo, and on the Collection in the British Museum (Natural History), London.* British Museum (Natural History), London, 324 p. https://doi.org/10.5962/bhl.title.55134

BAMFORD M. & PICKFORD M. 2021. — Stratigraphy, chronology and palaeontology of the Tertiary rocks of the Cheringoma Plateau, Mozambique. *Fossil Imprint* 77 (1): 187-213. https://doi.org/10.37520/fi.2021.014

BEADNELL H. J. L. 1902. — *A Preliminary Note on* Arsinoitherium zitteli *Beadnell, from the Upper Eocene Strata of Egypt*. Egyptian Survey Department, Public Works Ministry, Cairo: 1-4.

BENOIT J., ADNET S., EL MABROUK E., KHAYATI H., BEN HAJ ALI M., MARIVAUX L., MERZERAUD G., MERIGEAUD S., VIANEY-LIAUD M. & TABUCE R. 2013a. — Cranial Remain from Tunisia Provides New Clues for the Origin and Evolution of Sirenia (Mammalia, Afrotheria) in Africa, *in* FAHLMAN A. (ed.), *PLoS ONE* 8 (1): e54307. https://doi.org/10.1371/journal.pone.0054307

BENOIT J., MERIGEAUD S. & TABUCE R. 2013b. — Homoplasy in the ear region of Tethytheria and the systematic position of Embrithopoda (Mammalia, Afrotheria). *Geobios* 46 (5): 357-370. https://doi.org/10.1016/j.geobios.2013.07.002

BENOIT J., LYRAS G. A., SCHMITT A., NXUMALO M., TABUCE R., OBADA T., MARARSECUL V. & MANGER P. 2023. — Paleoneurology of the Proboscidea (Mammalia, Afrotheria): Insights from Their Brain Endocast and Labyrinth, *in* DOZO M. T., PAULINA-CARABAJAL A., MACRINI T. E. & WALSH S. (eds), *Paleoneurology of Amniotes*. Springer International Publishing, Cham: 579-644. https://doi.org/10.1007/978-3-031-13983-3_15

BILLET G., GERMAIN D., RUF I., MUIZON C. DE & HAUTIER L. 2013. — The inner ear of *Megatherium* and the evolution of the vestibular system in sloths. *Journal of Anatomy* 223 (6): 557-567. https://doi.org/10.1111/joa.12114

BILLET G., MUIZON C. DE, SCHELLHORN R., RUF I., LADEVÈZE S. & BERGQVIST L. 2015. — Petrosal and inner ear anatomy and allometry amongst specimens referred to Litopterna (Placentalia). *Zoological Journal of the Linnean Society* 173 (4): 956-987. https://doi.org/10.1111/zoj.12219

CHRISTIANSEN P. 2004. — Body size in proboscideans, with notes on elephant metabolism. *Zoological Journal of the Linnean Society* 140: 523-549. https://doi.org/10.1111/j.1096-3642.2004.00113.x

COURT N. 1990. — Periotic anatomy of *Arsinoitherium* (Mammalia, Embrithopoda) and its phylogenetic implications. *Journal of Vertebrate Paleontology* 10 (2): 170-182. https://doi.org/10.1080/02724634.1990.10011806

COURT N. 1992a. — Cochlea anatomy of *Numidotherium koholense*: auditory acuity in the oldest known proboscidean. *Lethaia* 25 (2): 211-215. https://doi.org/10.1111/j.1502-3931.1992.tb01385.x

COURT N. 1992b. — The skull of *Arsinoitherium* (Mammalia, Embrithopoda) and the higher order interrelationships of ungulates. *Palaeovertebrata* 22 (1): 1-43.

COURT N. 1994. — The periotic of *Moeritherium* (Mammalia, Proboscidea): homology or homoplasy in the ear region of Tethytheria McKenna, 1975? *Zoological Journal of the Linnean Society* 112 (1-2): 13-28. https://doi.org/10.1111/j.1096-3642.1994.tb00310.x

COURT N. & JAEGER J.-J. 1991. — Anatomy of the periotic bone in the Eocene proboscidean *Numidotherium koholense*: an example of parallel evolution in the inner ear of tethytheres. *Comptes rendus de l'Académie des sciences, Série 2, Mécanique, Physique, Chimie, Sciences de l'univers, Sciences de la Terre* 312 (5): 559-565. https://gallica.bnf.fr/ark:/12148/bpt6k5768142h

DAMUTH J. D. & MACFADDEN B. J. 1990a. — *Body Size in Mammalian Paleobiology: Estimation and Biological Implications*. Cambridge, Cambridge University Press., 397 p.

DAMUTH J. D. & MACFADDEN B. J. 1990b. — Problems in estimating body masses of archaic ungulates using dental measurements. *in* DAMUTH J. D. & MACFADDEN B. J. (eds), *Body Size in Mammalian Paleobiology: Estimation and Biological Implications*. Cambridge University Press, Cambridge: 229-253.

DOMNING D. P., HEAL G. J. & SORBI S. 2017. — *Libysiren sickenbergi*, gen. et sp. nov.: a new sirenian (Mammalia, Protosirenidae) from the middle Eocene of Libya. *Journal of Vertebrate Paleontology* 37 (2): e1299158. https://doi.org/10.1080/02724634.2017.1299158

EKDALE E. G. 2013. — Comparative anatomy of the bony labyrinth (inner ear) of placental mammals. *PLoS ONE* 8 (6): e66624. https://doi.org/10.1371/journal.pone.0066624

EKDALE E. G. & ROWE T. 2011. — Morphology and variation within the bony labyrinth of zhelestids (Mammalia, Eutheria) and other therian mammals. *Journal of Vertebrate Paleontology* 31 (3): 658-675. https://doi.org/10.1080/02724634.2011.557284

ENGELMAN R. K. 2022. — Occipital condyle width (OCW) is a highly accurate predictor of body mass in therian mammals. *BMC Biology* 20 (1): 37. https://doi.org/10.1186/s12915-021-01224-9

GHEERBRANT E. 2023. — Ancestral radiation of paenungulate mammals (Paenungulatomorpha) – new evidence from the Paleocene of Morocco. *Journal of Vertebrate Paleontology* 42 (5): e2197971. https://doi.org/10.1080/02724634.2023.2197971

GHEERBRANT E., SUDRE J., TASSY P., AMAGHZAZ M., BOUYA B. & IAROCHENE M. 2005. — Nouvelles données sur *Phosphatherium escuilliei* (Mammalia, Proboscidea) de l'Éocène inférieur du Maroc, apports à la phylogénie des Proboscidea et des ongulés lophodontes. *Geodiversitas* 27 (2): 239-333.

GHEERBRANT E., SCHMITT A., KOCSIS L. 2018. — Early African fossils elucidate the origin of embrithopod mammals. *Current Biology* 28: 2167-2173. https://doi.org/doi.org/10.1016/j.cub.2018.05.032

GHEERBRANT E., SCHMITT A. & BILLET G. 2020. — Petrosal and bony labyrinth morphology of the stem paenungulate mammal (Paenungulatomorpha) *Ocepeia daouiensis* from the Paleocene of Morocco. *Journal of Anatomy* 240 (4): 595-611. https://doi.org/10.1111/joa.13255

GHEERBRANT E., KHALDOUNE F., SCHMITT A. & TABUCE R. 2021. — Earliest embrithopod mammals (Afrotheria, Tethytheria) from the Early Eocene of Morocco: anatomy, systematics and phylogenetic significance. *Journal of Mammal Evolution* 28 (2): 245-283. https://doi.org/10.1007/s10914-020-09509-6

GOLOBOFF P. A. & CATALANO S. A. 2016. — TNT version 1.5, including a full implementation of phylogenetic morphometrics. *Cladistics* 32 (3): 221-238. https://doi.org/10.1111/cla.12160

LE VERGER K., HAUTIER L., GERBER S., BARDIN J., DELSUC F., GONZÁLEZ RUIZ L. R., AMSON E. & BILLET G. 2024. — Pervasive cranial allometry at different anatomical scales and variational levels in extant armadillos. *Evolution* 78 (3): 423-441. https://doi.org/10.1093/evolut/qpad214

LICHT A., MÉTAIS G., COSTER P., İBILIOĞLU D., OCAKOĞLU F., WESTERWEEL J., MUELLER M., CAMPBELL C., MATTINGLY S., WOOD M. C. & BEARD K. C. 2022. — Balkanatolia: The insular mammalian biogeographic province that partly paved the way to the Grande Coupure. *Earth-Science Reviews* 226: 103929. https://doi.org/10.1016/j.earscirev.2022.103929

MACPHEE R. D. E. & FORASIEPI A. M. 2022. — Re-Evaluating Cranial Pathways of the Internal Carotid Artery in Notoungulata (Mammalia, Panperissodactyla). *Ameghiniana* 59 (2): 141-161. https://doi.org/10.5710/AMGH.06.12.2021.3465

MACPHEE R. D., DEL PINO S. H., KRAMARZ A., FORASIEPI A. M., BOND M. & SULSER R. B. 2021. — Cranial morphology and phylogenetic relationships of *Trigonostylops wortmani*, an Eocene South American native ungulate. *Bulletin of the American Museum of Natural History* 449 (1): 1-183. https://doi.org/10.1206/0003-0090.449.1.1

MACRINI T. E., FLYNN J. J., CROFT D. A. & WYSS A. R. 2010. — Inner ear of a notoungulate placental mammal: anatomical description and examination of potentially phylogenetically informative characters. *Journal of Anatomy* 216 (5): 600-610. https://doi.org/10.1111/j.1469-7580.2010.01224.x

MALINZAK M. D., KAY R. F. & HULLAR T. E. 2012. — Locomotor head movements and semicircular canal morphology in primates. *Proceedings of the National Academy of Sciences* 109 (44): 17914-17919. https://doi.org/10.1073/pnas.1206139109

MEIN P. & PICKFORD M. 2018. — Reithroparamyine rodent from the Eocene of Namibia. *Communications of the Geological Survey of Namibia* 18: 38-47.

MORALES J. & PICKFORD M. 2018. — New *Namalestes* remains from the Ypresian/Lutetian of Black Crow, Namibia. *Communications of the Geological Survey of Namibia* 18: 72-80.

MUIZON C. DE, BILLET G., ARGOT C., LADEVÈZE S. & GOUSSARD F. 2015. — *Alcidedorbignya inopinata*, a basal pantodont (Placentalia, Mammalia) from the early Palaeocene of Bolivia: anatomy, phylogeny and palaeobiology. *Geodiversitas* 37 (4): 397-634. https://doi.org/10.5252/g2015n4a1

O'LEARY M. A. 2010. — An Anatomical and Phylogenetic Study of the Osteology of the Petrosal of Extant and Extinct Artiodactylans (Mammalia) and Relatives. *Bulletin of the American Museum of Natural History* 2010 (335): 1-206. https://doi.org/10.1206/335.1

PICKFORD M. 1986. — Première découverte d'une faune mammalienne terrestre paléogène d'Afrique sub-saharienne. *Comptes rendus de l'Académie des sciences. Série 2, Mécanique, Physique, Chimie, Sciences de l'univers, Sciences de la Terre* 302 (19): 1205-1210.

PICKFORD M. 2015a. — Cenozoic Geology of the Northern Sperrgebiet, Namibia, accenting the Palaeogene. *Communications of the Geological Survey of Namibia 16*: 10-104.

PICKFORD M. 2015b. — Large ungulates from the basal Oligocene of Oman: 1 – Embrithopoda. *Spanish Journal of Palaeontology* 30 (1): 33-42. https://doi.org/10.7203/sjp.30.1.17200

PICKFORD M. 2018a. — Additional material of *Namahyrax corvus* from the Ypresian/Lutetian of Black Crow, Namibia. *Communications of the Geological Survey of Namibia* 18: 81-86.

PICKFORD M. 2018b. — Characterising the zegdoumyid rodent *Tsaukhaebmys* from the Ypresian/Lutetian of Black Crow, Namibia. *Communications of the Geological Survey of Namibia* 19: 66-70.

PICKFORD M. 2018c. — First record of *Celtis* (Hackberry) from the Palaeogene of Africa, Sperrgebiet, Namibia. *Communications of the Geological Survey of Namibia* 19: 47-50.

PICKFORD M. 2018d. — Freshwater aquatic and aquaphile vertebrates from Black Crow (Ypresian/Lutetian, Namibia) and their palaeoenvironmental significance. *Communications of the Geological Survey of Namibia* 18: 26-37.

PICKFORD M. 2018e. — Land snails from the Ypresian/Lutetian of Black Crow, Namibia. *Communications of the Geological Survey of Namibia* 18: 19-25.

PICKFORD M. 2018f. — Mandible of *Namahyrax corvus* from the Eocene Black Crow Limestone, Namibia. *Communications of the Geological Survey of Namibia* 21: 32-39

PICKFORD M. 2019a. — Adapisoriculidae from the Southern Hemisphere. *Communications of the Geological Survey of Namibia* 21: 26-31.

PICKFORD M. 2019b. — New Chrysochloridae (Mammalia) from the middle Eocene of Black Crow, Namibia. *Communications of the Geological Survey of Namibia* 21: 40-47.

PICKFORD M. 2019c. — Tiny Tenrecomorpha (Mammalia) from the Eocene of Black Crow, Namibia. *Communications of the Geological Survey of Namibia* 21: 15-25.

PICKFORD M., SENUT B., MORALES J., MEIN P. & SANCHEZ I. 2008a. — Mammalia from the Lutetian of Namibia. *Memoirs of the Geological Survey of Namibia* 20: 465-514.

PICKFORD M., SENUT B., MORALES J. & SANCHEZ I. M. 2008b. — Fossiliferous Cainozoic Carbonates of the Northern Sperrgebiet. *Memoirs of the Geological Survey of Namibia* 20: 25-42.

RASMUSSEN D. T. & GUTIERREZ M. 2009. — A mammalian fauna from the late Oligocene of northwestern Kenya. *Palaeontographica Abteilung A* 288: 1-52. https://doi.org/10.1127/pala/288/2009/1

RUF I., VOLPATO V., ROSE K. D., BILLET G., MUIZON C. DE & LEHMANN T. 2016. — Digital reconstruction of the inner ear of *Leptictidium auderiense* (Leptictida, Mammalia) and North American leptictids reveals new insight into leptictidan locomotor agility. *Paläontologische Zeitschrift* 90 (1): 153-171. https://doi.org/10.1007/s12542-015-0276-2

SANDERS W. J., KAPPELMAN J. & RASMUSSEN D. T. 2004. — New large-bodied mammals from the late Oligocene site of Chilga, Ethiopia. *Acta Palaeontologica Polonica* 49 (3): 365-392.

SANDERS W. J., GHEERBRANT E., HARRIS J. M., SAEGUSA H. & DELMER C. 2010. — Proboscidea, *in* WERDELIN L. & SANDERS W. J. (eds), *Cenozoic Mammals of Africa*. University of California Press, pp. 161–151.

SAVAGE R. J. G., DOMNING D. P. & THEWISSEN J. G. 1994. — Fossil Sirenia of the West Atlantic and Caribbean Region. V. the Most Primitive Known Sirenian, *Prorastomus sirenoides* Owen, 1855. *Journal of Vertebrate Paleontology* 14 (3): 427-449. https://doi.org/10.1080/02724634.1994.10011569

SCHMITT A. 2016. — *La région de l'oreille osseuse chez les Proboscidiens (Mammalia) : Anatomie, fonction, évolution*. PhD Thesis, École doctorale des sciences de la nature et de l'homme, Muséum national d'Histoire naturelle, Paris, 473 p.

SCOTESE C. R., SONG H., MILLS B. J. W. & VAN DER MEER D. G. 2021. — Phanerozoic paleotemperatures: The earth's changing climate during the last 540 million years. *Earth-Science Reviews* 215: 103503. https://doi.org/10.1016/j.earscirev.2021.103503

SEGALL W. 1970. — Morphological parallelisms of the bulla and auditory ossicles in some insectivores and marsupials. *Fieldiana Zoology* 51: 169-205. https://doi.org/10.5962/bhl.title.2899

SPOOR F. & ZONNEVELD F. 1998. — Comparative review of the human bony labyrinth. *American Journal of Physical Anthropology*107 (S27): 211-251. https://doi.org/10.1002/(SICI)1096-8644(1998)107:27+<211::AID-AJPA8>3.0.CO;2-V

SPOOR F., GARLAND T., KROVITZ G., RYAN T. M., SILCOX M. T. & WALKER A. 2007. — The primate semicircular canal system and locomotion. *Proceedings of the National Academy of Sciences* 104 (26): 10808-10812. https://doi.org/10.1073/pnas.0704250104

STANHOPE M. J., WADDELL V. G., MADSEN O., DE JONG W., HEDGES S. B., CLEVEN G. C., KAO D. & SPRINGER M. S. 1998. — Molecular evidence for multiple origins of Insectivora and for a new order of endemic African insectivore mammals. *Proceedings of the National Academy of Sciences* 95 (17): 9967-9972. https://doi.org/10.1073/pnas.95.17.9967

TASSY P. 1981. — Le crâne de *Moeritherium* (Proboscidea, Mammalia) de l'Éocène de Dor El Talha (Libye) et le problème de la classification phylogénétique du genre dans les Tethytheria McKenna, 1975. *Bulletin du Muséum national d'Histoire naturelle, série 4, section C, Sciences de la Terre, Paléontologie, Géologie, Minéralogie* 3 (1): 87-147. https://www.biodiversitylibrary.org/page/55659745

VIALLE N., MERZERAUD G., DELMER C., FEIST M., JIQUEL S., MARIVAUX L., RAMDARSHAN A., VIANEY-LIAUD M., ESSID E. M., MARZOUGUI W., AMMAR H. K. & TABUCE R. 2013. — Discovery of an embrithopod mammal (*Arsinoitherium*?) in the late Eocene of Tunisia. *Journal of African Earth Sciences* 87: 86-92. https://doi.org/10.1016/j.jafrearsci.2013.07.010

VOIT M. 1909. — Das Primordialcranium des Kaningchens. *Anatomy and Embryology* 38 (3): 425-616.

WAIBL, H., GASSE, H., CONSTANTINESCU, G., HASHIMOTO, Y. & SIMOENS, P. 2005 – Nomina Anatomica Veterinaria. V^th^ Edition, Editorial Committee, International Committee on Veterinary Gross Anatomical Nomenclature (I.C.V.G.A.N): Hannover, Columbia, Gent, Sapporo, 166 p.

WEST C. D. 1985. — The relationship of the spiral turns of the cochlea and the length of the basilar membrane to the range of audible frequencies in ground dwelling mammals. *The Journal of the Acoustical Society of America* 77 (3): 1091-1101. https://doi.org/10.1121/1.392227

WIBLE J. R. 2008. — On the Cranial Osteology of the Hispaniolan Solenodon, *Solenodon paradoxus* Brandt, 1833 (Mammalia, Lipotyphla, Solenodontidae). *Annals of Carnegie Museum* 77 (3): 321-402. https://doi.org/10.2992/0097-4463-77.3.321

WIBLE J. R. 2010. — Petrosal anatomy of the nine-banded armadillo, *Dasypus novemcinctus* Linnaeus, 1758 (Mammalia, Xenarthra, Dasypodidae). *Annals of Carnegie Museum* 79 (1): 1-29. https://doi.org/10.2992/007.079.0101

WIBLE J. R. 2012. — The Ear Region of the Aardvark, *Orycteropus afer* (Pallas, 1766) (Mammalia, Placentalia, Tubulidentata). *Annals of Carnegie Museum* 80 (2): 115-146. https://doi.org/10.2992/007.080.0202

WIBLE J. 2022. — Petrosal and cranial vascular system of the early Eocene palaeoryctid *Eoryctes melanus* from northwestern Wyoming, USA. *Acta Palaeontologica Polonica* 67. https://doi.org/10.4202/app.00916.2021

WIBLE J. R. & SHELLEY S. L. 2020. — Anatomy of the Petrosal and Middle Ear of the Brown Rat, *Rattus norvegicus* (Berkenhout, 1769) (Rodentia, Muridae). *Annals of Carnegie Museum* 86 (1): 1-35. https://doi.org/10.2992/007.086.0101

ZALMOUT I. S., SANDERS W. J., MACLATCHY L. M., GUNNELL G. F., AL-MUFARREH Y. A., ALI M. A., NASSER A.-A. H., AL-MASARI A. M., AL-SOBHI S. A., NADHRA A. O., MATARI A. H., WILSON J. A. & GINGERICH P. D. 2010. — New Oligocene primate from Saudi Arabia and the divergence of apes and Old World monkeys. *Nature* 466 (7304): 360-364. https://doi.org/10.1038/nature09094

Submitted on 22 April 2024;
accepted on 26 August 2024;
published on 22 May 2025.

APPENDIX 1. — Characters modified in the phylogenetic matrix of Gheerbrant (2023). *, character modified; **, character recoded; ***, character added.

#	Description	Modification
27*	Molar crown height	State 1, "Unilateral hypsodonty" divided in two states: state 1, unilateral labial hypsodonty; and state 2, unilateral lingual hypsodonty.
32**	Posmetacristid	Crivadiatherium, state 1, presence of a distinct postmetacristid.
48**	M3 relative size	Crivadiatherium, state 2, M3 significantly larger than M2.
60**	Coronoid foramen	Desmostylia, state 0, coronoid foramen absent.
74**	P2 number of roots	Arsinoitherium, state 0, P2 with 2 roots
75*	P2 protocone	State 2 added, protocone very small, but still distinct as an independent cuspule; Namatherium and Arsinoitherium, state 2
90*	P4 lophs	One state added: state 0, no loph; state 1, one loph; state 2, two lophs.
131**	Number of lingual roots of M3	Namatherium, state 2, 3 roots (Pickford *et al.* 2008a).
145**	Anterior margin of choanae	Namatherium, state 0, at M3 mid-level
157**	Orbit position	Namatherium, state 2, orbit above M2; Arsinoitherium, state 0, orbit above M3
189*	Periotic, fenestra vestibuli shape	Stapedial ratio limit between oval shape (state 0) and round (state 1) = 1.6 instead 1.8 (Benoit *et al.* 2013b).
190 (Gheerbrant's 2023 numbering)	Relative position of fenestra_ cochleae and fenestra_vestibuli	Character of Gheerbrant (2023) deleted from matrix because it is not informative (see text).
190*	Periotic: Fenestra cochleae and cochlear aqueduct	3 states instead 2 (one intermediate state added). State 0: Fenestra cochleae and cochlear aqueduct present and well separated; state 1: Fenestra cochleae (and part of the cochlear fossula) and cochlear aqueduct present but partly merged; state 2: Fenestra cochleae and cochlear aqueduct merged in a unique perilymphatic duct. Character additive.
192***	Periotic: Medial caudal tympanic process	State 0, weak, non-inflated; state 1, inflated.
198***	Periotic, inner ear	Shape (section) of the crural limb of the semicircular canals: state 0: cylindrical; state 1 more or less flattened. This is character 33 of Benoit *et al.* (2013b) and character 21 of Benoit *et al.* (2023).
199***	Periotic, inner ear	Shape of semicircular canals in section: state 0, semicircular canals thin (thickness ratio <3); state 1 semicircular canal thick (thickness ratio =<3). This is character 22 of Benoit *et al.* (2023).
200***	Foramen magnum	State 0 enclosed by supraoccipital and exoccipitals; state 1 enclosed only by exoccipitals.

APPENDIX 2. — Character-taxon matrix analysed (modified from Gheerbrant 2023). The matrix includes 10 uninformative characters, and 38 additive characters. https://doi.org/10.7934/P5894

APPENDIX 3. — Composite reconstruction of the skull of *Namatherium blackcrowense* Pickford, Senut, Morales, Mein & Sanchez, 2008 combining the holotype GSN BC 13'08 and specimen GSN BC 21'19. 3D digital model made from surface scanning. Each isolated bone of GSN BC 21'19 is modelised separately and can be hidden from the reconstruction. The missing parts are reconstructed by mirror-imaging (pdf file). https://doi.org/10.7934/P5894

APPENDIX 4. — Table of data and measurements for the embrithopods *Stylolophus* Gheerbrant, 2018, *Namatherium* Pickford, Senut, Morales, Mein & Sanchez, 2008 and *Arsinoitherium* Beadnell, 1902 used for Figure 12.

Taxon	BM, g	ASCR, mm	LSCR, mm	PSCR, mm	SCR, mm	logBM	logSCR	References
Stylolophus major Gheerbrant, 2021	88 000	3.260	2.290	3.130	2.89	4.944	0.461	Gheerbrant *et al.* (2021)
Arsinoitherium zitelli Beadnell, 1902	1 000 000	4.400	3.180	4.070	3.88	6.000	0.589	Benoit *et al.* (2013b); Christiansen (2004); Sanders *et al.* (2010)
Namatherium blackcrowense (left bony lab.)	345 000	3.685	3.005	3.453	3.38	5.538	0.529	present study